



January 2019

# Earthquake Loading Effects On The Buckling Of Liquid Filled Cylindrical Storage Tanks

Hailey Johnson

Follow this and additional works at: <https://commons.und.edu/theses>

---

## Recommended Citation

Johnson, Hailey, "Earthquake Loading Effects On The Buckling Of Liquid Filled Cylindrical Storage Tanks" (2019). *Theses and Dissertations*. 2465.

<https://commons.und.edu/theses/2465>

This Thesis is brought to you for free and open access by the Theses, Dissertations, and Senior Projects at UND Scholarly Commons. It has been accepted for inclusion in Theses and Dissertations by an authorized administrator of UND Scholarly Commons. For more information, please contact [zeinebyousif@library.und.edu](mailto:zeinebyousif@library.und.edu).

EARTHQUAKE LOADING EFFECTS ON THE BUCKLING OF LIQUID FILLED  
CYLINDRICAL STORAGE TANKS

by

Hailey Marie Johnson  
Bachelor of Science, University of North Dakota, 2017

A Thesis

Submitted to the Graduate Faculty

of the

University of North Dakota

in partial fulfillment of the requirements

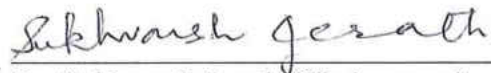
for the degree of

Master of Science

Grand Forks, North Dakota

May  
2019

This thesis, submitted by Hailey Johnson in partial fulfillment of the requirements for the Degree of Master of Science from the University of North Dakota, has been read by the Faculty Advisory Committee under whom the work has been done and is hereby approved.



Dr. Sukhvarsh Jerath (Chairperson)



Dr. Daba Gedafa



Dr. Nabil Suleiman

This thesis is being submitted by the appointed advisory committee as having met all of the requirements of the School of Graduate Studies at the University of North Dakota and is hereby approved.



Chris Nelson  
Dean of the School of Graduate Studies

5/2/19

Date

## PERMISSION

Title            Earthquake Loading Effects on the Buckling of Liquid Filled Cylindrical Storage Tanks

Department    Civil Engineering

Degree         Master of Science

In presenting this thesis in partial fulfillment of the requirements for a graduate degree from the University of North Dakota, I agree that the library of this University shall make it freely available for inspection. I further agree that permission for extensive copying for scholarly purposes may be granted by the professor who supervised my thesis work or, in his absence, by the Chairperson of the department or the dean of the School of Graduate Studies. It is understood that any copying or publication or other use of this thesis or part thereof for financial gain shall not be allowed without my written permission. It is also understood that due recognition shall be given to me and to the University of North Dakota in any scholarly use which may be made of any material in my thesis.

Hailey Johnson  
4/22/2019

## TABLE OF CONTENTS

ACKNOWLEDGEMENTS.....	xi
ABSTRACT.....	xii
CHAPTER I: INTRODUCTION.....	1
1.1 Introduction.....	1
1.2 Literature Review.....	2
CHAPTER II: THEORY .....	5
CHAPTER III: MODEL.....	7
3.1 Geometry and Materials.....	7
3.2 ANSYS Modeling.....	8
3.3 Verification of the Models.....	9
CHAPTER IV: STATIC BUCKLING ANALYSIS .....	13
4.1 Eigenvalue Buckling Analysis.....	13
4.2 Nonlinear Static Buckling Analysis.....	16
CHAPTER V: MODAL ANALYSIS.....	29
CHAPTER VI: TRANSIENT DYNAMIC BUCKLING ANALYSIS .....	43
6.1 Definition and Method.....	43
6.2 Earthquake Data.....	45
6.3 Results.....	46
CHAPTER VII: CONCLUSION.....	61

REFERENCES ..... 63

## LIST OF TABLES

Table 1: Geometry of the Cylindrical Tanks .....	7
Table 2: Theoretical and Finite Element Analysis Buckling Stress Comparison.....	12
Table 3: Eigenvalue Buckling Loads.....	14
Table 4: Results from Eigenvalue and Nonlinear Buckling Analyses.....	16
Table 5: First Natural Frequencies for 90% Filled Tanks .....	30
Table 6: Model 1 Natural Frequencies at 90% Filled.....	31
Table 7: Model 2 Natural Frequencies at 90% Filled.....	32
Table 8: Model 3 Natural Frequencies at 90% Filled.....	33
Table 9: Model 4 Natural Frequencies at 90% Filled.....	34
Table 10: Model 5 Natural Frequencies at 90% Filled.....	35
Table 11: Model 6 Natural Frequencies at 90% Filled.....	36
Table 12: Model 7 Natural Frequencies at 90% Filled.....	37
Table 13: Model 8 Natural Frequencies at 90% Filled.....	38
Table 14: Model 9 Natural Frequencies at 90% Filled.....	39
Table 15: Model 10 Natural Frequencies at 90% Filled.....	40
Table 16: Model 11 Natural Frequencies at 90% Filled.....	41
Table 17: Model 12 Natural Frequencies at 90% Filled.....	42
Table 18: First Natural Frequencies and Mass Coefficients.....	45
Table 19: Dynamic Buckling of the 90% Filled Cylindrical Tanks .....	47

## TABLE OF FIGURES

Figure 1: States of Equilibrium (Ghosh et al. 2019).....	5
Figure 2: Cylindrical Tank Diagram.....	8
Figure 3: SHELL 181 (“SHELL 181” 2015).....	9
Figure 4: SOLID 186 (“SOLID 186” 2015).....	9
Figure 5: Finite Element Model of Pin-Pin End Tank with Compressive Load.....	10
Figure 6: Finite Element Model with Lateral Load .....	13
Figure 7: Eigenvalue Buckling Shape for Model 1 .....	15
Figure 8: Eigenvalue Buckling Shape for Model 10 .....	15
Figure 9: Load-Deflection Curve of Maximum Deflection Node for Model 1 .....	17
Figure 10: Post-Buckling Deflected Shape of Model 1 .....	17
Figure 11: Load-Deflection Curve of Maximum Deflection Node for Model 2 .....	18
Figure 12: Post-Buckling Deflected Shape of Model 2 .....	18
Figure 13: Load-Deflection Curve of Maximum Deflection Node for Model 3 .....	19
Figure 14: Post-Buckling Deflected Shape of Model 3 .....	19
Figure 15: Load-Deflection Curve of Maximum Deflection Node for Model 4 .....	20
Figure 16: Post-Buckling Deflected Shape of Model 4 .....	20
Figure 17: Load-Deflection Curve of Maximum Deflection Node for Model 5 .....	21
Figure 18: Post-Buckling Deflected Shape of Model 5 .....	21
Figure 19: Load-Deflection Curve of Maximum Deflection Node for Model 6 .....	22



Figure 20: Post-Buckling Deflected Shape of Model 6 .....	22
Figure 21: Load-Deflection Curve of Maximum Deflection Node for Model 7 .....	23
Figure 22: Post-Buckling Deflected Shape of Model 7 .....	23
Figure 23: Load-Deflection Curve of Maximum Deflection Node for Model 8 .....	24
Figure 24: Post-Buckling Deflected Shape of Model 8 .....	24
Figure 25: Load-Deflection Curve of Maximum Deflection Node for Model 9 .....	25
Figure 26: Post-Buckling Deflected Shape of Model 9 .....	25
Figure 27: Load-Deflection Curve of Maximum Deflection Node for Model 10 .....	26
Figure 28: Post-Buckling Deflected Shape of Model 10 .....	26
Figure 29: Load-Deflection Curve of Maximum Deflection Node for Model 11 .....	27
Figure 30: Post-Buckling Deflected Shape of Model 11 .....	27
Figure 31: Load-Deflection Curve of Maximum Deflection Node for Model 12 .....	28
Figure 32: Post-Buckling Deflected Shape of Model 12 .....	28
Figure 33: Model 1 First Mode 90% Filled (Scale 50:1).....	31
Figure 34: Model 2 First Mode 90% Filled (Scale 300:1).....	32
Figure 35: Model 3 First Mode 90% Filled (Scale 50:1).....	33
Figure 36: Model 4 First Mode 90% Filled (Scale 400:1).....	34
Figure 37: Model 5 First Mode 90% Filled (Scale 125:1).....	35
Figure 38: Model 6 First Mode 90% Filled (Scale 500:1).....	36
Figure 39: Model 7 First Mode 90% Filled (Scale 125:1).....	37

Figure 40: Model 8 First Mode 90% Filled (Scale 700:1).....	38
Figure 41: Model 9 First Mode 90% Filled (Scale 150:1).....	39
Figure 42: Model 10 First Mode 90% Filled (Scale 700:1).....	40
Figure 43: Model 11 First Mode 90% Filled (Scale 300:1).....	41
Figure 44: Model 12 First Mode 90% Filled (Scale 1500:1).....	42
Figure 45: Accelerogram of the First Eight Seconds of the El Centro Earthquake.....	46
Figure 46: Effective Earthquake Force (Chopra 2012) .....	46
Figure 47: Dynamic Buckling Capacities from the Transient Analysis .....	48
Figure 48: Pseudo Equilibrium Paths for the Critical Node of Model 1 .....	49
Figure 49: Shell Deformation of Model 1 .....	49
Figure 50: Pseudo Equilibrium Paths for the Critical Node of Model 2 .....	50
Figure 51: Shell Deformation of Model 2 .....	50
Figure 52: Pseudo Equilibrium Paths for the Critical Node of Model 3 .....	51
Figure 53: Shell Deformation of Model 3 .....	51
Figure 54: Pseudo Equilibrium Paths for the Critical Node of Model 4 .....	52
Figure 55: Shell Deformation of Model 4 .....	52
Figure 56: Pseudo Equilibrium Paths for the Critical Node of Model 5 .....	53
Figure 57: Shell Deformation of Model 5 .....	53
Figure 58: Pseudo Equilibrium Paths for the Critical Node of Model 6 .....	54
Figure 59: Shell Deformation of Model 6 .....	54

Figure 60: Pseudo Equilibrium Paths for the Critical Node of Model 7 .....	55
Figure 61: Shell Deformation of Model 7 .....	55
Figure 62: Pseudo Equilibrium Paths for the Critical Node of Model 8 .....	56
Figure 63: Shell Deformation of Model 8 .....	56
Figure 64: Pseudo Equilibrium Paths for the Critical Node of Model 9 .....	57
Figure 65: Shell Deformation of Model 9 .....	57
Figure 66: Pseudo Equilibrium Paths for the Critical Node of Model 10 .....	58
Figure 67: Shell Deformation of Model 10 .....	58
Figure 68: Pseudo Equilibrium Paths for the Critical Node of Model 11 .....	59
Figure 69: Shell Deformation of Model 11 .....	59
Figure 70: Pseudo Equilibrium Paths for the Critical Node of Model 12 .....	60
Figure 71: Shell Deformation of Model 12 .....	60

## ACKNOWLEDGEMENTS

I wish to express my sincere appreciation to my advisor, Dr. Sukhvarsh Jerath, and my committee members, Dr. Daba Gedafa and Dr. Nabil Suleiman, for their support and guidance throughout my Master of Science program at the University of North Dakota.

## ABSTRACT

This thesis studied twelve liquid filled cylindrical storage tanks to determine the static buckling loads, as well as the dynamic buckling loads when subjected to earthquake loading. The geometries of the cylindrical tanks were investigated with height-to-diameter ratios of 0.5, 0.75, 1.0, 1.25, 1.5, and 2.0 and with diameter-to-thickness ratios of 520.83 and 1,041.67. Each cylindrical tank modeled had a constant thickness of 0.36 inches. ANSYS Workbench was used to create a finite element analysis of each cylindrical tank. A transient dynamic buckling analysis was performed on each model in order to determine the dynamic buckling load of the cylindrical tanks, filled to 90% height with water and subjected to horizontal earthquake excitations. Analysis of the results show when either height-to-diameter ratios or diameter-to thickness ratios increase, the dynamic buckling loads of the cylindrical tanks decrease.

## **CHAPTER I: INTRODUCTION**

### **1.1 Introduction**

Above-ground liquid storage tanks can be damaged during earthquakes. Earthquakes apply an acceleration to the storage tanks and the liquids inside, which can lead to numerous failures, including buckling of the tank wall or possibly collapse. These storage tanks contain liquids that range from food products to hazardous materials. When the liquid storage tanks are damaged during an earthquake, the fluid inside can leak and cause major damage to the surrounding areas. In Turkey, the Kocaeli earthquake caused damage to oil storage tanks and created fires that burned for one week. The Kocaeli earthquake also caused the floating roofs of the oil storage tanks to sink (Zama 2003).

The buckling of cylindrical storage tanks caused by horizontal earthquake acceleration is the focus of this study. Finite element analysis was used to investigate the static and dynamic buckling behaviors of cylindrical liquid storage tanks subjected to earthquake loads. All finite element analysis modeling and analyzing was completed using ANSYS Workbench (ANSYS® 19.1). Twelve different geometries were chosen for comparison of the cylindrical liquid storage tanks, which include height-to-diameter ratios of 0.5, 0.75, 1.0, 1.25, 1.5, and 2.0 with diameter-to-thickness ratios of 520.83 and 1,041.67. The thickness was set to a constant 0.36 inches for each cylindrical tank model. The empty storage tanks were analyzed using eigenvalue buckling and nonlinear static buckling. Each cylindrical tank was filled to 90% height with liquid and subjected to the El Centro earthquake (University of Berkley 2016) in order to perform a nonlinear dynamic buckling analysis.

Chapter 2 discusses the finite element analysis model, geometries and materials, and the verification of the ANSYS models using the theoretical values to determine the adequacy of the ANSYS models. Chapter 3 shows the static buckling analysis, which includes eigenvalue buckling analysis and nonlinear static buckling analysis for each model. Chapter 4 presents modal analysis to find the natural frequencies and mode shapes for each finite element analysis model. Chapter 5 presents dynamic buckling using the transient buckling analysis. Chapter 6 discusses the results of this study.

## **1.2 Literature Review**

Many researchers have studied the buckling behaviors of cylindrical tanks. Earthquakes have exposed the vulnerabilities of cylindrical shell structures when subjected to seismic loading. Research has been done on cylindrical shells under axial compression, empty and filled cylindrical storage tanks under dynamic loading, and the interactions between cylindrical storage tanks and the liquid inside.

The buckling of thin cylindrical shells under axial compression has been covered by multiple researchers. Timoshenko studied thin cylindrical shells with symmetrical and asymmetrical loading and presented how to find the bending moments and deformation of the shell structures (Timoshenko and Woinowsky 1959). Mandal and Calladine studied the effects of self-weight buckling on open-top cylindrical shells using finite element analysis to determine the nonlinear buckling load behavior. It was found that there is a post-buckling-plateau load, which relates to the experimental buckling loads, due to the static determinacy of the cylindrical shells (Mandal and Calladine 2000).

The effects of fluid inside a cylindrical tank during seismic loading was studied by Housner, who researched dynamic behavior of water-filled tanks. He concluded that the cylindrical tanks have two motions when a dynamic load is applied. When a fluid filled cylindrical tank is first subjected to a dynamic load, both the tank and the fluid inside act as one structure and move together in the same pattern. The motion of the tank walls then begin to excite the water and an oscillating force from the water on the tank is exerted (Housner 1963).

Another study on the hydrodynamic pressures acting on the walls of cylindrical tanks was done by Butnaru, Sandru, Furis, and Cretu. The tanks studied were of different geometries, but had the same volume. This study compared the tanks using a ratio of the tank radius to the fluid depth. From this study, it was found that the fundamental period and the first ten periods of oscillation of the fluid can differ and these variances impact the overturning effect of the cylindrical tanks (Butnaru et al. 2016).

Meskouris, Holtschoppen, Butenweg, and Rosin studied the interactions of the tank wall and the fluid inside, in order to create easier formulas for the future. The convective pressure (sloshing), the rigid impulsive pressure, rigid tank movement with the ground, the flexible impulsive pressure, and the combined vibration of flexible cylindrical tanks with the fluid were studied (Meskouris et al. 2011). This research has provided information that is able to help create easier finite element analysis models.

Jerath and Lee researched dynamic buckling loads of cylindrical tanks, using ANSYS computer software. The cylindrical tanks chosen were compared by height-to-diameter ratios and they found the cylindrical tanks resisted a larger earthquake loading when the height-to-diameter ratio was decreased (Jerath and Lee 2015). Roopkumdee and Jerath also studied the effects of height-to-diameter and diameter-to-thickness ratios of cylindrical tanks. The height-to-diameter



ratio and the diameter-to thickness ratio were both found to affect the cylindrical tanks. When either was decreased the cylindrical tanks had a higher buckling tolerance to earthquake loading (Roopkumdee and Jerath 2017).

## CHAPTER II: THEORY

A structure is unstable when the structural members can no longer resist the compression loadings applied to it. Two limit states exist when designing a new structure. Strength limit states consider the maximum load a structure can carry without failure. Serviceability limit state deals with the structures ability to perform under normal service conditions. The definitions of stability can be categorized into stable equilibrium, unstable equilibrium, and neutral equilibrium. Stable equilibrium is when an object is subjected to a force and when the force is removed, the object will return to its initial position. The object is in unstable equilibrium if the force is removed and the object continues to displace infinitesimally. Neutral equilibrium is when an object is subjected to a force and the object attains a new equilibrium position (Chen and Lui 1987).

Figure 1 explains the concept of stability using a ball on a surface.

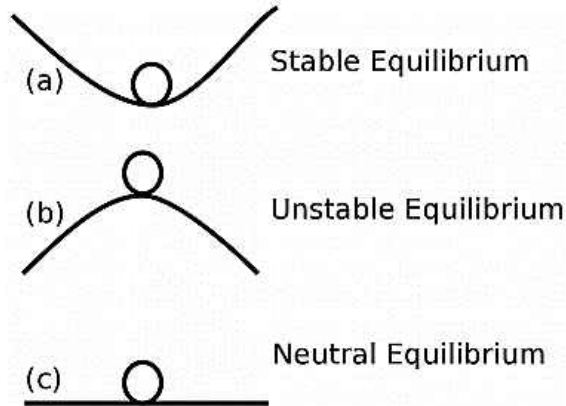


Figure 1: States of Equilibrium (Ghosh et al. 2019)

Two categories of stability are considered when structures are subjected to compressive loads. Bifurcation of equilibrium occurs when a structure under an increasing compressive load will deflect in the direction of the load until reaching its critical load, then the deflection will change to a new direction. Asymmetric and symmetric bifurcations are determined based on the post-buckling behavior path. Stable symmetric bifurcation occurs when the load capacity

increases after buckling. If the load capacity decreases after buckling, then the stability is described as unstable symmetric bifurcation. The other category of stability with a compressive load is limit-load instability. Limit-load instability is when there is only a single mode of deflection throughout loading, from start to the limit. The system will reach a limit load and will jump from one equilibrium to another nonadjacent equilibrium (Chen and Lui 1987).

Stability is analyzed to find the critical conditions using multiple methods: bifurcation approach, energy approach, and dynamic approach. Bifurcation approach uses the eigenvalues of the system's stiffness matrix to indicate the critical conditions and the eigenvectors to indicate the displaced configurations, only in a geometrically perfect system. The energy approach uses the total potential energy of the system to determine the critical conditions, in an elastic system. The final method is the dynamic approach, which is used in an elastic system. The critical load, using the dynamic approach, is found "as the level of external applied force when the motion ceases to be bounded" (Chen and Lui 1987).

## CHAPTER III: MODEL

### 3.1 Geometry and Materials

For this project, twelve different cylindrical tanks were modeled and analyzed in order to determine their buckling behaviors. The cylindrical tanks all shared a thickness of 0.36 inches and were open on the top. The height-to-diameter (H/D) ratios modeled were 0.5, 0.75, 1.0, 1.25, 1.5, and 2.0. The diameter-to-thickness ratios were 520.8 and 1041.7. The cylindrical tank dimensions are listed in Table 1. A diagram of a cylindrical tank is shown in Figure 2.

*Table 1: Geometry of the Cylindrical Tanks*

	<b>H/D</b>	<b>D/t</b>	<b>t</b>	<b>H</b>	<b>D</b>
<b>Model 1</b>	0.50	520.8	0.36 in (9.14 mm)	93.75 in (2.38 m)	187.5 in (4.76 m)
<b>Model 2</b>	0.50	1,041.7	0.36 in (9.14 mm)	187.50 in (4.76 m)	375.0 in (9.53 m)
<b>Model 3</b>	0.75	520.8	0.36 in (9.14 mm)	140.63 in (3.57 m)	187.5 in (4.76 m)
<b>Model 4</b>	0.75	1,041.7	0.36 in (9.14 mm)	281.25 in (7.14 m)	375.0 in (9.53 m)
<b>Model 5</b>	1.00	520.8	0.36 in (9.14 mm)	187.50 in (4.76 m)	187.5 in (4.76 m)
<b>Model 6</b>	1.00	1,041.7	0.36 in (9.14 mm)	375.00 in (9.53 m)	375.0 in (9.53 m)
<b>Model 7</b>	1.25	520.8	0.36 in (9.14 mm)	234.38 in (5.95 m)	187.5 in (4.76 m)
<b>Model 8</b>	1.25	1,041.7	0.36 in (9.14 mm)	468.75 in (11.91 m)	375.0 in (9.53 m)
<b>Model 9</b>	1.50	520.8	0.36 in (9.14 mm)	281.25 in (7.14 m)	187.5 in (4.76 m)
<b>Model 10</b>	1.50	1,041.7	0.36 in (9.14 mm)	562.50 in (14.29 m)	375.0 in (9.53 m)
<b>Model 11</b>	2.00	520.8	0.36 in (9.14 mm)	375.00 in (9.53 m)	187.5 in (4.76 m)
<b>Model 12</b>	2.00	1,041.7	0.36 in (9.14 mm)	750.00 in (19.05 m)	375.0 in (9.53 m)

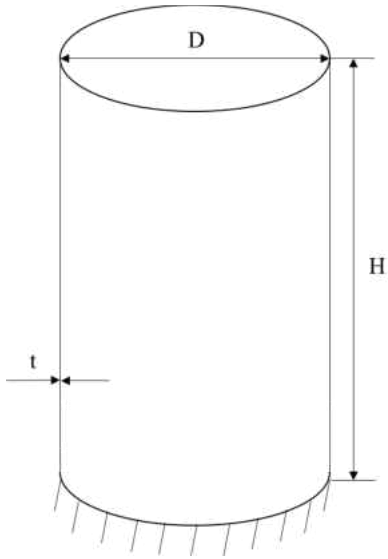


*Figure 2: Cylindrical Tank Diagram*

The material used to model the cylindrical tanks was structural steel with a Modulus of Elasticity of 29,000,000 psi (200,000 MPa), a mass density of 15.232 slugs/ft<sup>3</sup> (7,850 kg/m<sup>3</sup>), and Poisson's ratio of 0.3. The yield stress of the steel was 50,000 psi (344.74 MPa) and the tangent modulus was 2,000,000 psi (13,789.51 MPa). The fluid inside the tank was modeled as water and has a mass density of 1.9403 slugs/ft<sup>3</sup> (1,000 kg/m<sup>3</sup>) and a bulk modulus of 300,000 psi (2,068.43 MPa).

### **3.2 ANSYS Modeling**

ANSYS Workbench, a computer program, was used for all finite element analysis. SHELL181 element was used for the steel cylindrical storage tanks and SOLID186 element was used to model the liquid inside the cylindrical tanks. SHELL181 is a four-node element with six degrees of freedom at each node. These degrees of freedom are translation in the x, y, and z directions and rotation about the x, y, and z axes. SOLID186 is a twenty-node element with three degrees of freedom at each node, including translation in the x, y, and z direction. The liquid element was modeled to be detached from the tank walls and have coinciding nodes normal to

the interface. Each model was created using half-symmetry, which reduces the time needed to compute each model. Figure 3 and 4 display the location of the nodes for each element and the coordinate system.

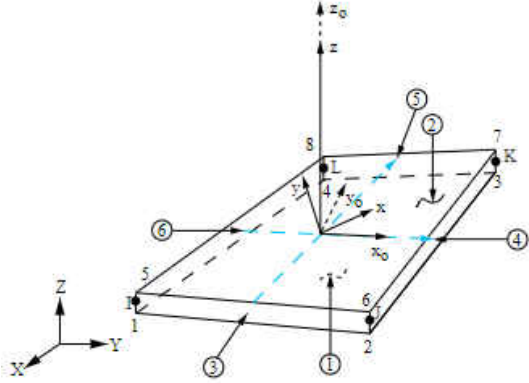


Figure 3: SHELL 181 (“SHELL 181” 2015)

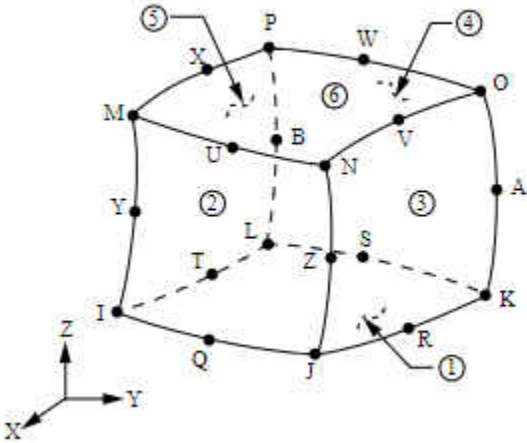


Figure 4: SOLID 186 (“SOLID 186” 2015)

### 3.3 Verification of the Models

Finite element models accuracy is checked by comparing the critical eigenvalue buckling load stresses to the theoretical values. The equation for theoretical buckling stress of a pin-pin ended cylindrical shell is given in Equation 1.

$$\sigma_{cr} = \frac{E}{\sqrt{3(1-\nu^2)}} \left( \frac{t}{R} \right) \quad (1)$$

- Where:
- $\sigma_{cr}$ : theoretical static buckling stress, psi (MPa)
  - E: modulus of elasticity of the structural steel, psi (MPa)
  - $\nu$ : Poisson's ratio of the structural steel
  - t: thickness of the cylindrical shell, in. (mm)
  - R: radius of the cylindrical shell, in. (mm)

Using ANSYS, a compressive load of 1 lb/in (0.018 kg/mm) was applied to the top of the pin-pin ended cylindrical tank, shown in Figure 5.

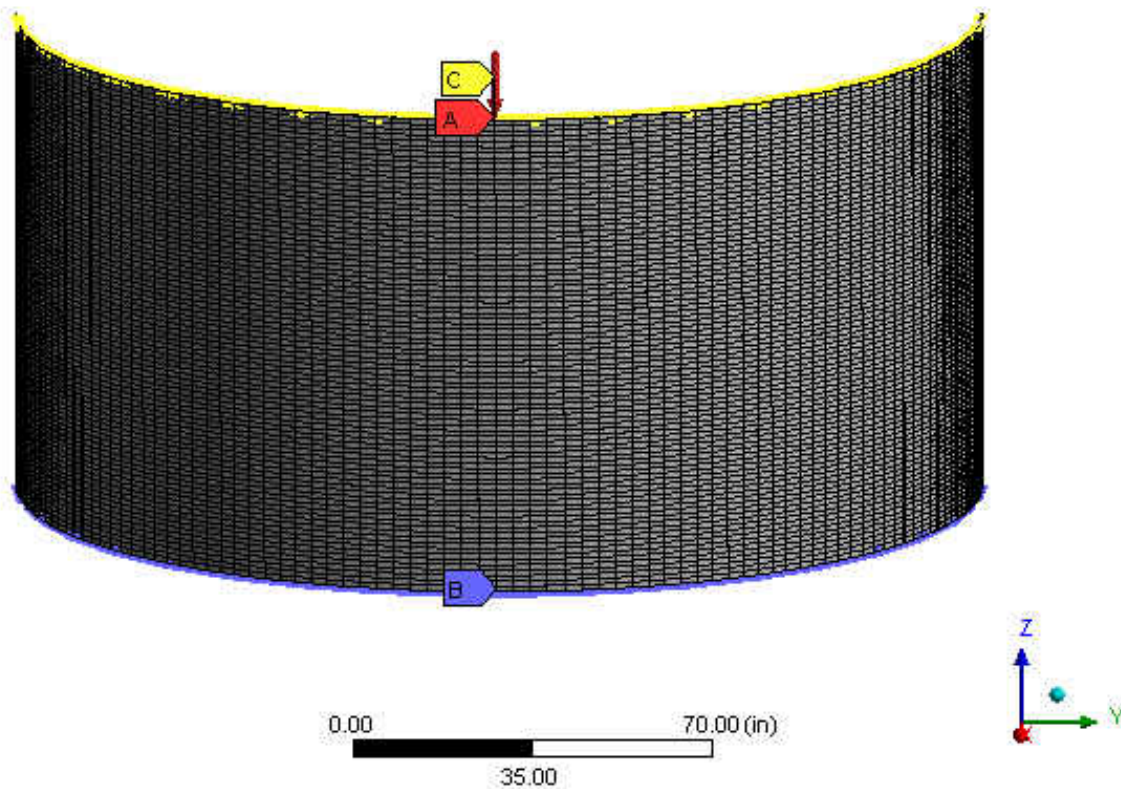


Figure 5: Finite Element Model of Pin-Pin End Tank with Compressive Load

From the ANSYS simulation, the buckling stress can be found using Equation 2.

$$\sigma_{cr (ANSYS)} = \frac{\text{Multiplier}}{t} \quad (2)$$

For example, using Model 1:

Theoretical buckling stress:

$$\sigma_{cr} = \frac{29,000,000 \text{ psi}}{\sqrt{3(1 - (0.3)^2)}} \left( \frac{0.36 \text{ in}}{93.75 \text{ in}} \right) = 67,398.14 \text{ psi (464.67 MPa)}$$

Finite element analysis buckling stress:

$$\sigma_{cr (ANSYS)} = \frac{24,388 \text{ lb/in}}{0.36 \text{ in}} = 67,744.44 \text{ psi (467.06 MPa)}$$

Error between theoretical and finite element analysis buckling stress:

$$\frac{67,744.44 - 67,398.14}{67,398.14} \times 100\% = 0.51\%$$

The comparison between the theoretical and critical eigenvalue buckling values are displayed in Table 2.



Table 2: Theoretical and Finite Element Analysis Buckling Stress Comparison

Model	t	Multiplier	Buckling Stress		Error (%)
			Theoretical	ANSYS	
1	0.36	24,388 lb/in (4,271,103 N/m)	67,398 psi (465 MPa)	67,744 psi (467 MPa)	0.51
2	0.36	12,239 lb/in (2,143,433 N/m)	33,699 psi (232 MPa)	33,997 psi (234 MPa)	0.88
3	0.36	24,501 lb/in (4,290,893 N/m)	67,398 psi (465 MPa)	68,058 psi (469 MPa)	0.98
4	0.36	12,379 lb/in (2,167,951 N/m)	33,699 psi (232 MPa)	34,386 psi (237 MPa)	2.04
5	0.36	24,682 lb/in (4,322,592 N/m)	67,398 psi (465 MPa)	68,561 psi (473 MPa)	1.73
6	0.36	12,581 lb/in (2,203,327 N/m)	33,699 psi (232 MPa)	34,947 psi (241 MPa)	3.70
7	0.36	24,937 lb/in (4,367,250 N/m)	67,398 psi (465 MPa)	69,269 psi (478 MPa)	2.78
8	0.36	12,830 lb/in (2,246,935 N/m)	33,699 psi (232 MPa)	35,639 psi (246 MPa)	5.76
9	0.36	24,954 lb/in (4,370,228 N/m)	67,398 psi (465 MPa)	69,317 psi (478 MPa)	2.85
10	0.36	12,747 lb/in (2,232,399 N/m)	33,699 psi (232 MPa)	35,408 psi (244 MPa)	5.07
11	0.36	24,739 lb/in (4,332,574 N/m)	67,398 psi (465 MPa)	68,719 psi (474 MPa)	1.96
12	0.36	12,608 lb/in (2,208,056 N/m)	33,699 psi (232 MPa)	35,022 psi (241 MPa)	3.93

The error between the theoretical buckling stress and the finite element analysis stress was calculated. For these cylindrical tanks, the error was below 6% which means that the models are acceptable.

## CHAPTER IV: STATIC BUCKLING ANALYSIS

### 4.1 Eigenvalue Buckling Analysis

The eigenvalue buckling analysis was assumed as linear elastic buckling behavior. For this study, the cylindrical tanks were modeled with half-symmetry. The cylindrical tanks were modeled with a fixed support on the bottom of the tank and free at the top of the tank. A unit force (1.0 lbf) applied to the top of the tank in the y-direction of the Cartesian coordinate system. The ANSYS model with the load and fixed support is shown in Figure 6. ANSYS computed a multiplier for the lateral linear buckling load. Due to half-symmetry, in order to obtain the eigenvalue buckling load, the multiplier obtained was multiplied by two. The eigenvalue buckling loads that were found for the cylindrical tanks are shown in Table 3.

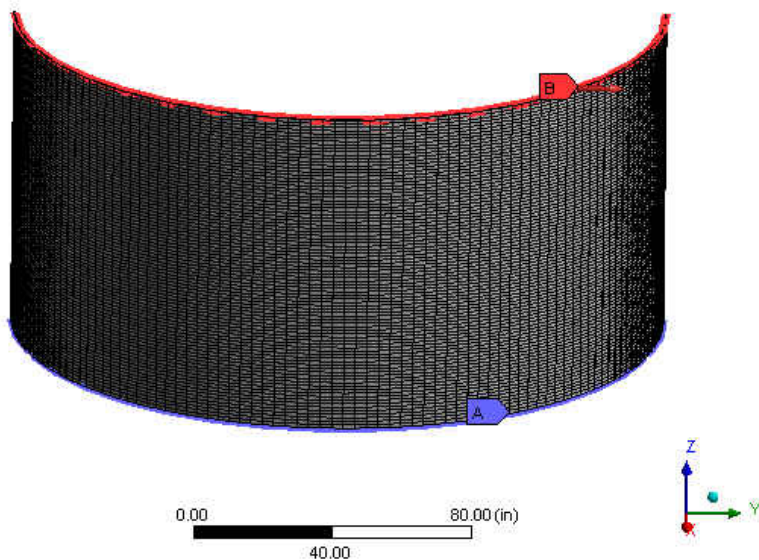


*Figure 6: Finite Element Model with Lateral Load*

Table 3: Eigenvalue Buckling Loads

<b>Model</b>	<b>H/D</b>	<b>D/t</b>	<b>Multiplier</b>	<b>Eigenvalue Buckling Load</b>
<b>1</b>	0.5	520.83	98,644 lb (438,966 N)	197,288 lb (877,932 N)
<b>2</b>	0.5	1,041.67	67,044 lb (298,346 N)	134,088 lb (596,692 N)
<b>3</b>	0.75	520.83	96,189 lb (428,041 N)	192,378 lb (856,082 N)
<b>4</b>	0.75	1,041.67	65,905 lb (293,277 N)	131,810 lb (586,555 N)
<b>5</b>	1.0	520.83	95,268 lb (423,943 N)	190,536 lb (847,885 N)
<b>6</b>	1.0	1,041.67	65,475 lb (291,364 N)	130,950 lb (582,728 N)
<b>7</b>	1.25	520.83	94,849 lb (422,078 N)	189,698 lb (844,156 N)
<b>8</b>	1.25	1,041.67	65,291 lb (290,545 N)	130,582 lb (581,090 N)
<b>9</b>	1.5	520.83	94,648 lb (421,184 N)	189,296 lb (842,367 N)
<b>10</b>	1.5	1,041.67	65,222 lb (290,238 N)	130,444 lb (580,476 N)
<b>11</b>	2.0	520.83	94,542 lb (420,712 N)	189,084 lb (841,424 N)
<b>12</b>	2.0	1,041.67	65,254 lb (290,380 N)	130,508 lb (580,761 N)

The eigenvalues found using ANSYS were used to indicate the upper limit for the nonlinear static buckling analysis. Figures 7 and 8 show the buckling mode shape for the maximum and minimum eigenvalue buckling loads. The highest buckling load was in Model 1 and the lowest buckling load was in Model 10.

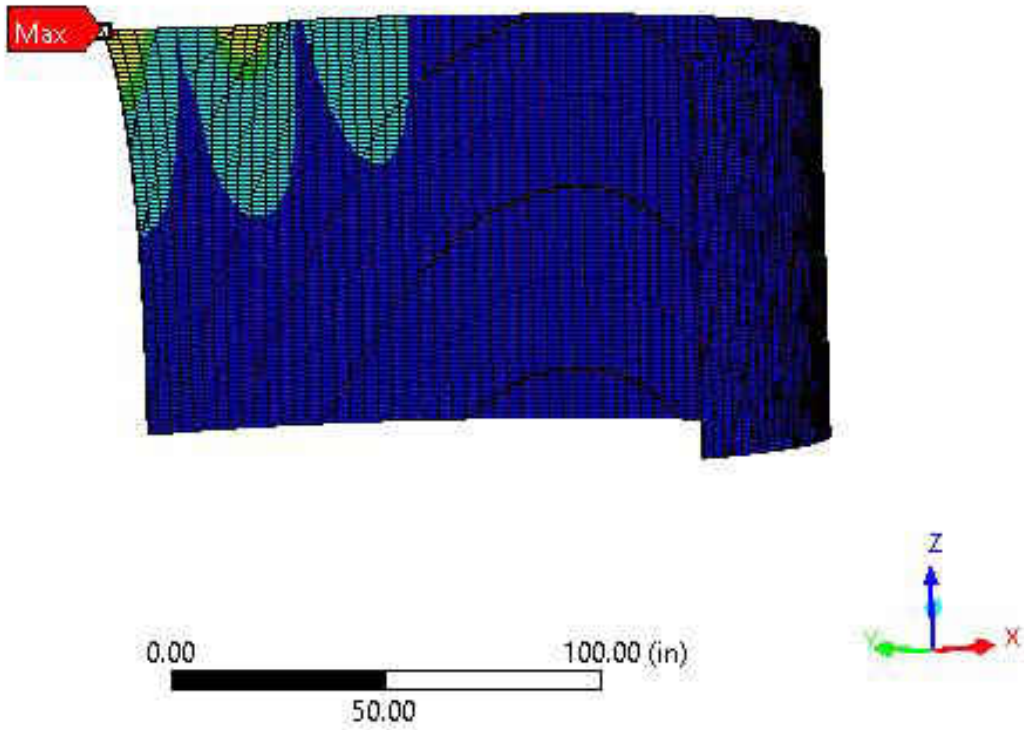


Figure 7: Eigenvalue Buckling Shape for Model 1

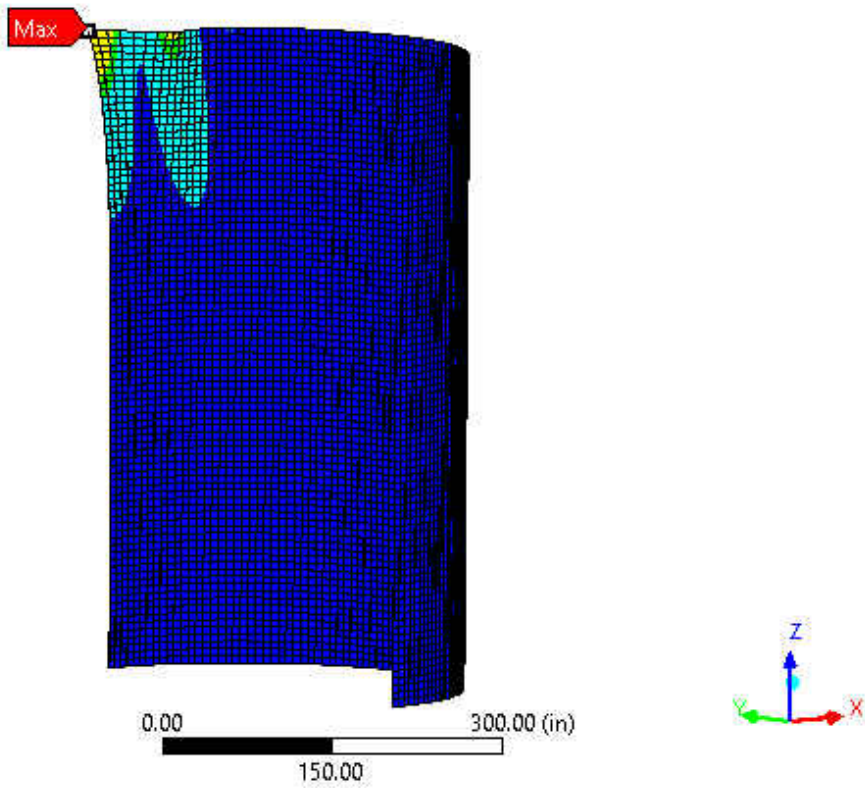


Figure 8: Eigenvalue Buckling Shape for Model 10

## 4.2 Nonlinear Static Buckling Analysis

Nonlinear buckling analysis was done in order to find a more exact value for the static buckling load of the cylindrical tanks. The eigenvalue buckling load values found in the previous section were used to determine the upper limit of the nonlinear static buckling analysis.

The twelve cylindrical tanks were modeled in ANSYS with half symmetry, a fixed support on the bottom, and free at the top. Large deflection was applied to the models, allowing the program to increase the load continuously until the tank is no longer stable. A lateral load of 90% of the eigenvalue buckling load was applied to the top of the cylindrical tank. If the model would not converge, the lateral load value was decreased until it would converge. A load deflection curve was then created using the node with the maximum load displacement. Table 4 shows the difference between the eigenvalue and nonlinear buckling loads. The data from Table 4 shows that the nonlinear buckling was within 85% and 90% of the eigenvalue buckling load, as expected.

*Table 4: Results from Eigenvalue and Nonlinear Buckling Analyses*

<b>Model</b>	<b>H/D</b>	<b>D/t</b>	<b>Eigenvalue Buckling</b>	<b>Nonlinear Buckling</b>	<b>% Difference</b>
<b>1</b>	0.5	520.83	197,288 lb (877,932 N)	172,506 lb (767,652 N)	14.37
<b>2</b>	0.5	1,041.67	134,088 lb (596,692 N)	115,002 lb (511,759 N)	16.60
<b>3</b>	0.75	520.83	192,378 lb (856,082 N)	174,004 lb (774,318 N)	10.56
<b>4</b>	0.75	1,041.67	131,810 lb (586,555 N)	112,008 lb (498,436 N)	17.68
<b>5</b>	1.0	520.83	190,536 lb (847,885 N)	170,008 lb (756,536 N)	12.07
<b>6</b>	1.0	1,041.67	130,950 lb (582,728 N)	115,000 lb (511,750 N)	13.87
<b>7</b>	1.25	520.83	189,698 lb (844,156 N)	166,754 lb (742,055 N)	13.76
<b>8</b>	1.25	1,041.67	130,582 lb (581,090 N)	117,000 lb (516,236 N)	11.61
<b>9</b>	1.5	520.83	189,296 lb (842,367 N)	166,754 lb (742,055 N)	13.52
<b>10</b>	1.5	1,041.67	130,444 lb (580,476 N)	115,000 lb (511,750 N)	13.43
<b>11</b>	2.0	520.83	189,084 lb (841,424 N)	165,000 lb (734,250 N)	14.60
<b>12</b>	2.0	1,041.67	130,508 lb (580,761 N)	115,800 lb (515,310 N)	12.70

## Model 1

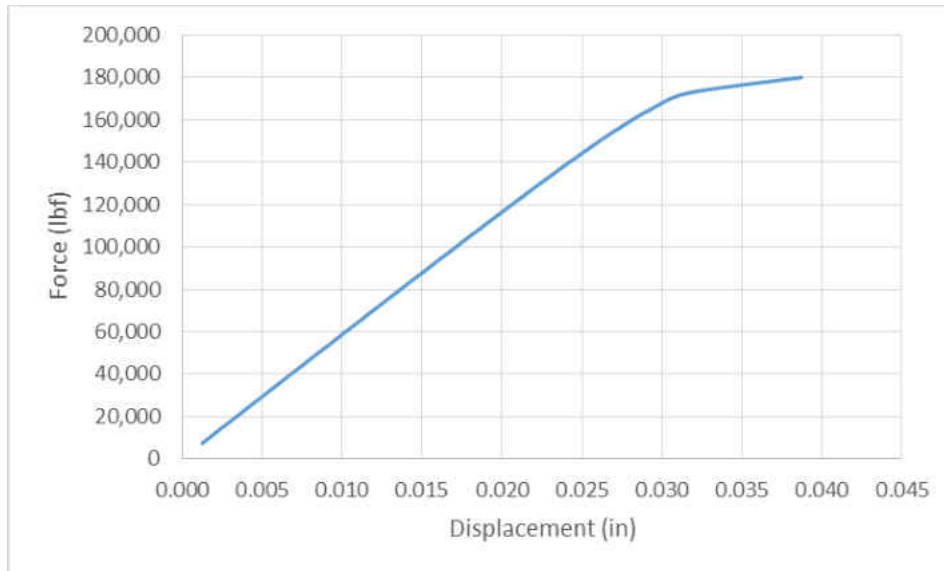


Figure 9: Load-Deflection Curve of Maximum Deflection Node for Model 1

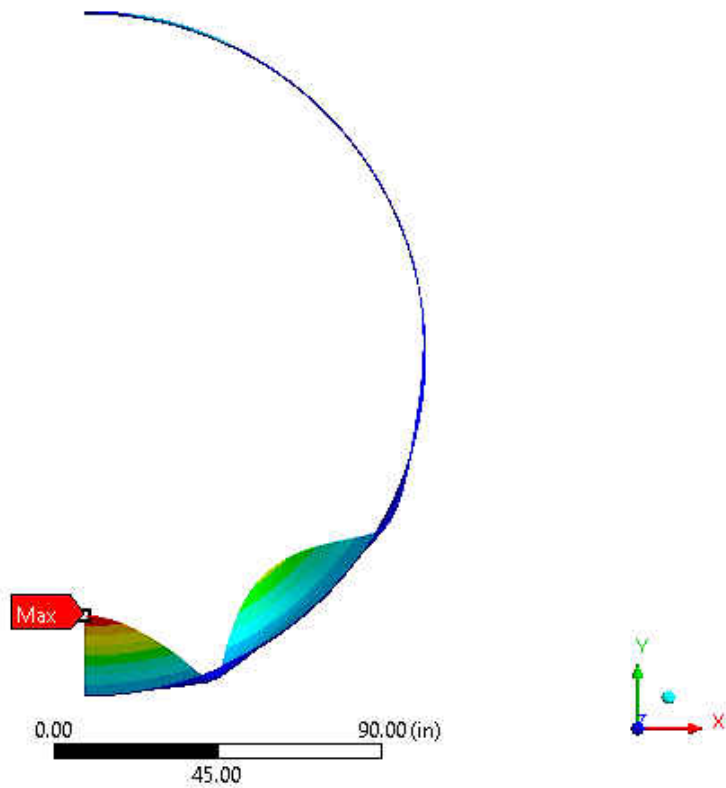


Figure 10: Post-Buckling Deflected Shape of Model 1

**Model 2**

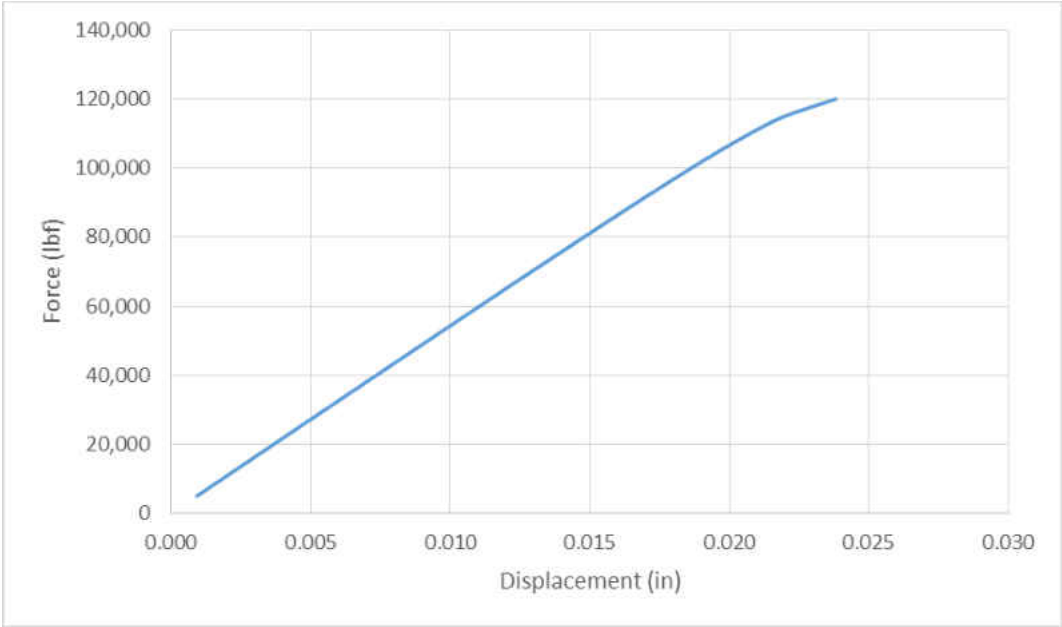


Figure 11: Load-Deflection Curve of Maximum Deflection Node for Model 2

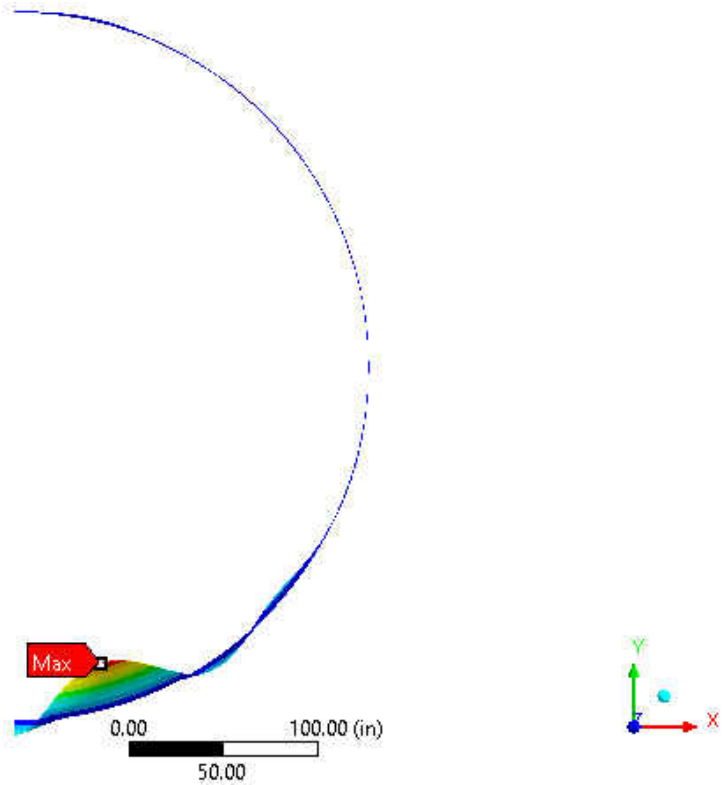


Figure 12: Post-Buckling Deflected Shape of Model 2

**Model 3**

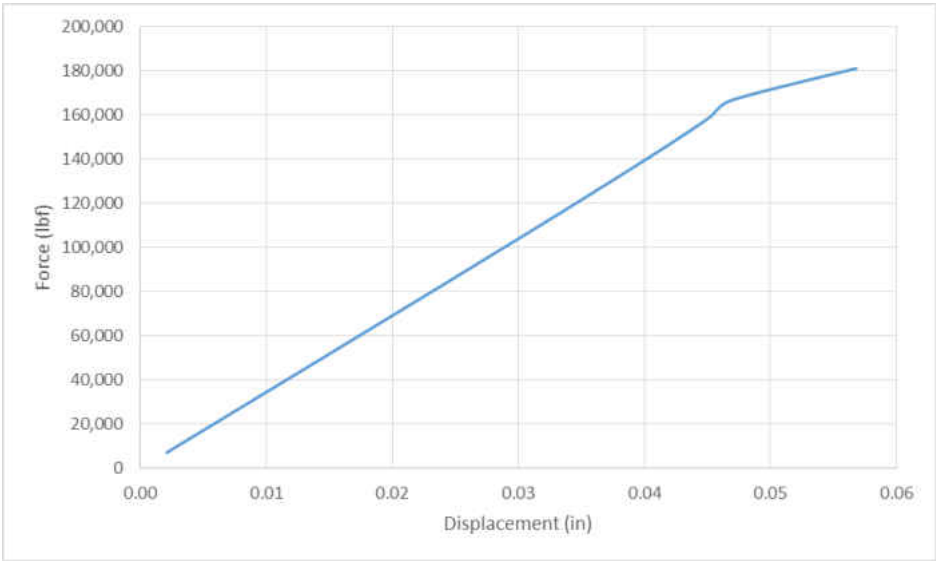


Figure 13: Load-Deflection Curve of Maximum Deflection Node for Model 3

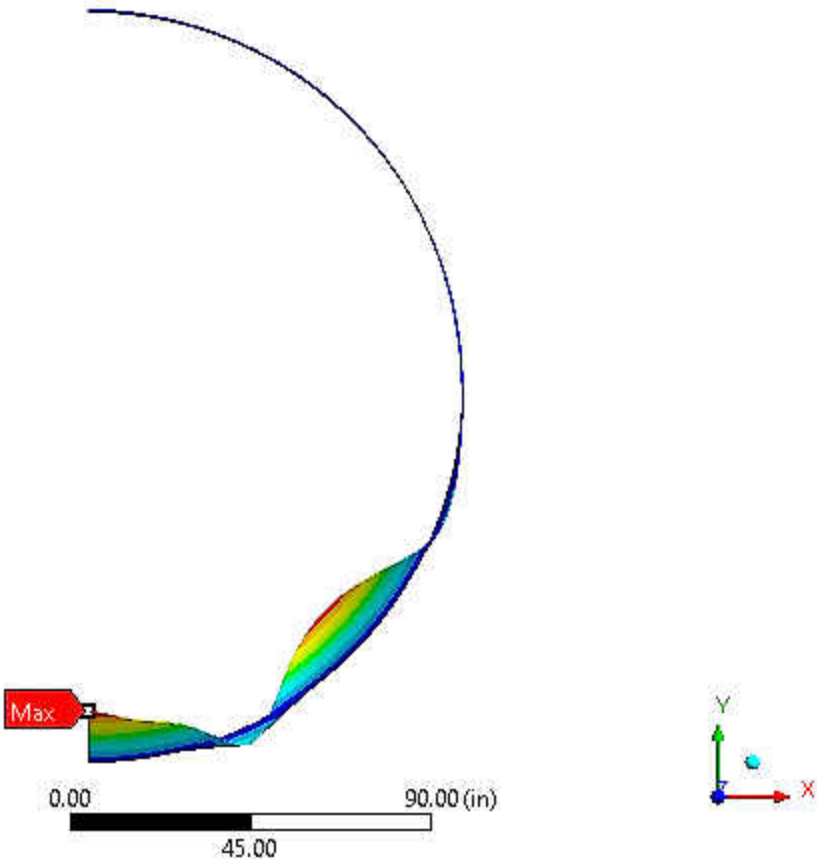


Figure 14: Post-Buckling Deflected Shape of Model 3



## Model 4

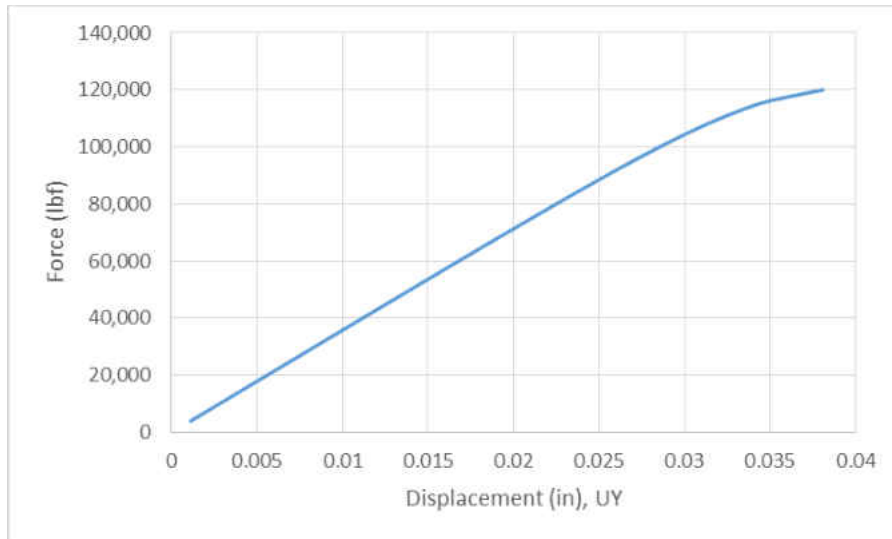


Figure 15: Load-Deflection Curve of Maximum Deflection Node for Model 4

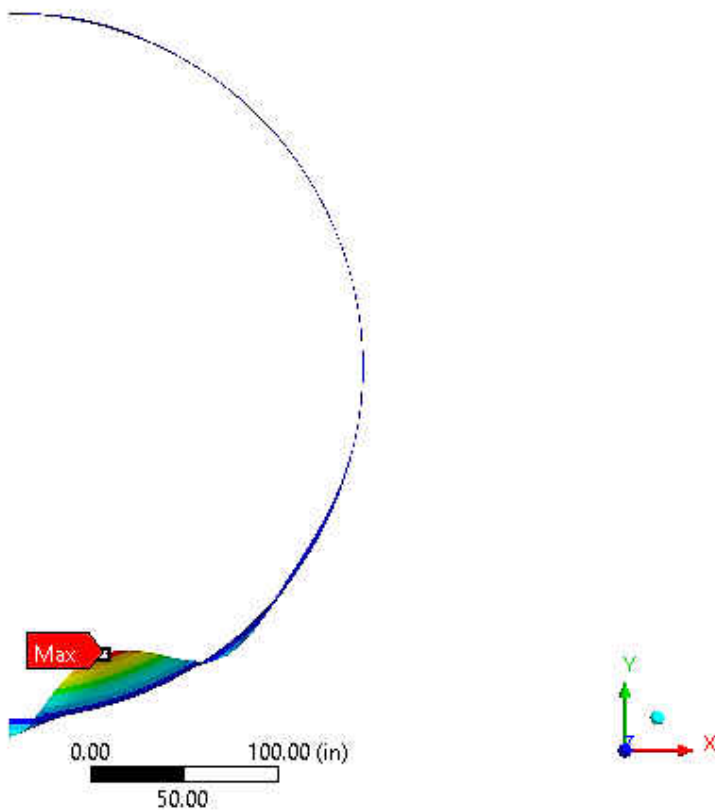


Figure 16: Post-Buckling Deflected Shape of Model 4

**Model 5**

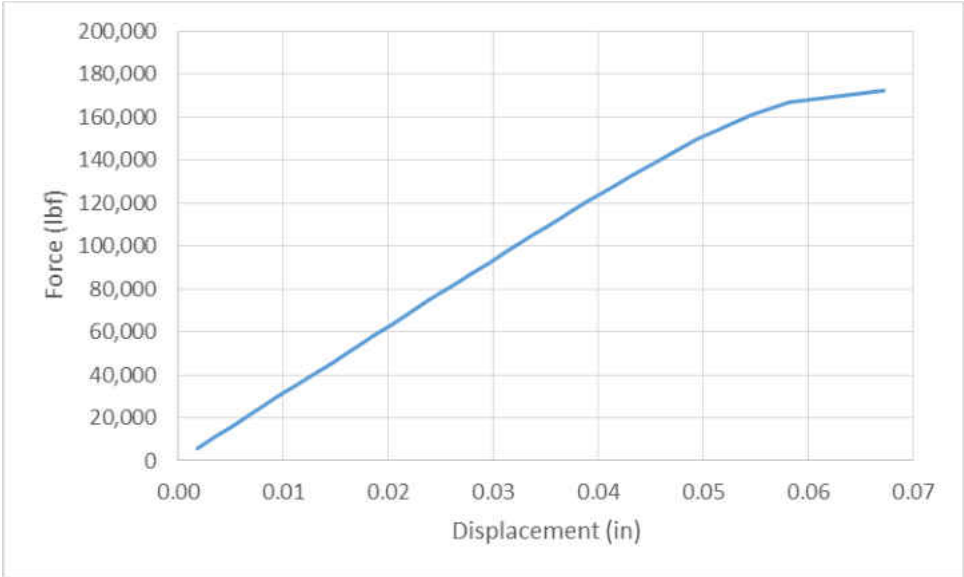


Figure 17: Load-Deflection Curve of Maximum Deflection Node for Model 5

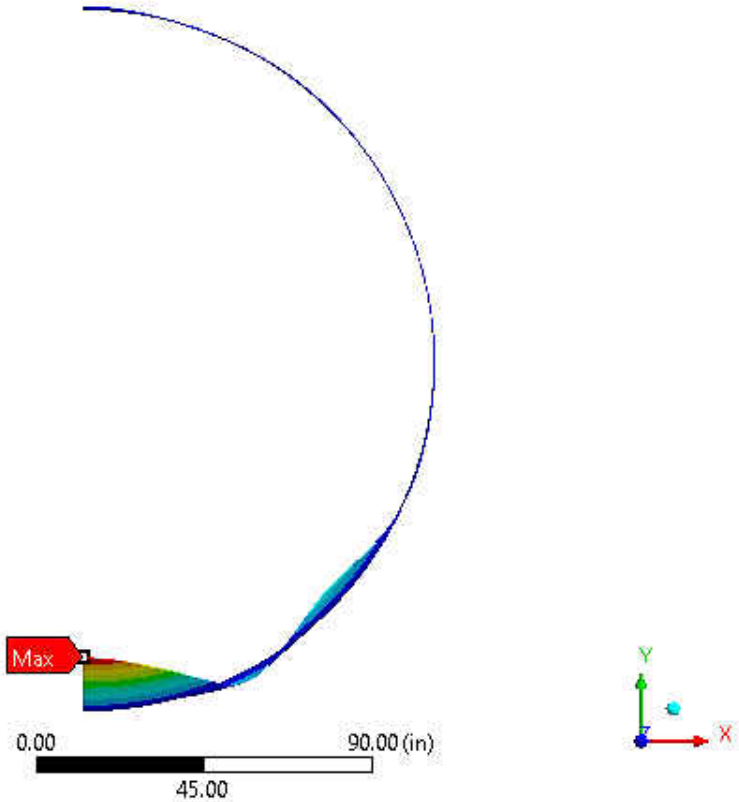
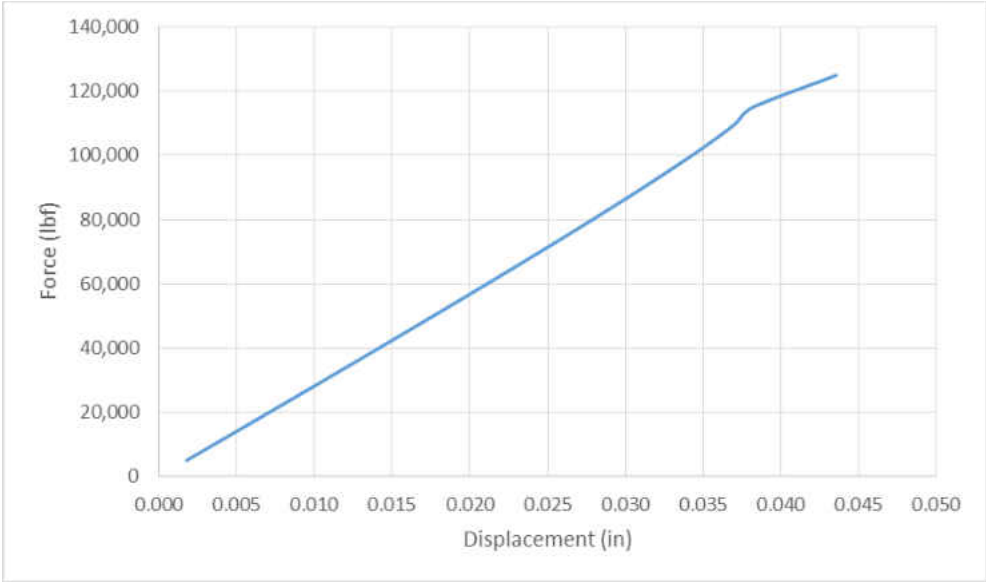
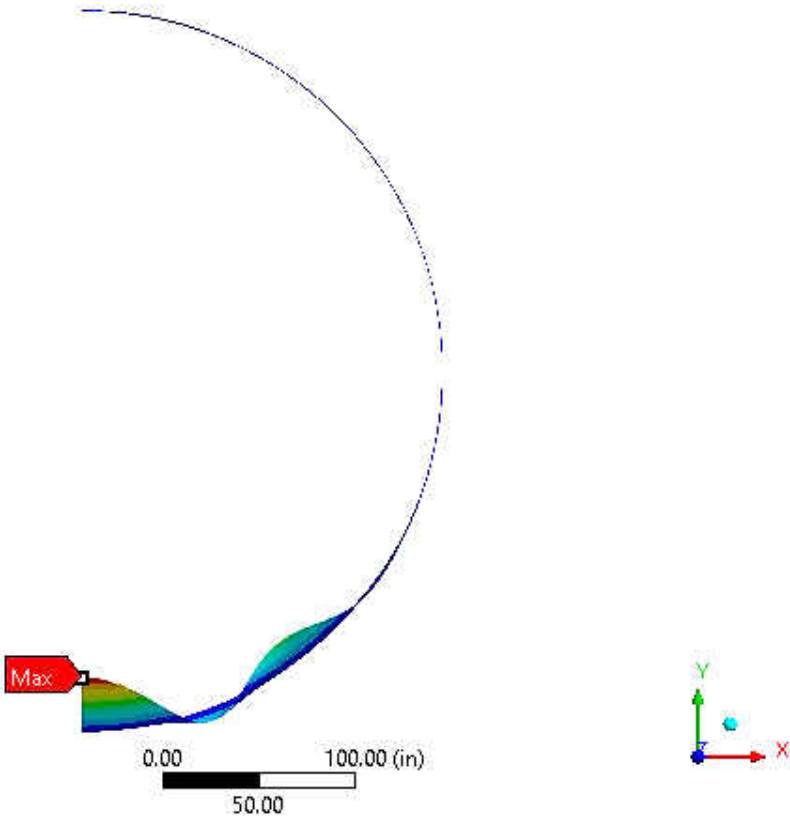


Figure 18: Post-Buckling Deflected Shape of Model 5

**Model 6**



*Figure 19: Load-Deflection Curve of Maximum Deflection Node for Model 6*



*Figure 20: Post-Buckling Deflected Shape of Model 6*

**Model 7**

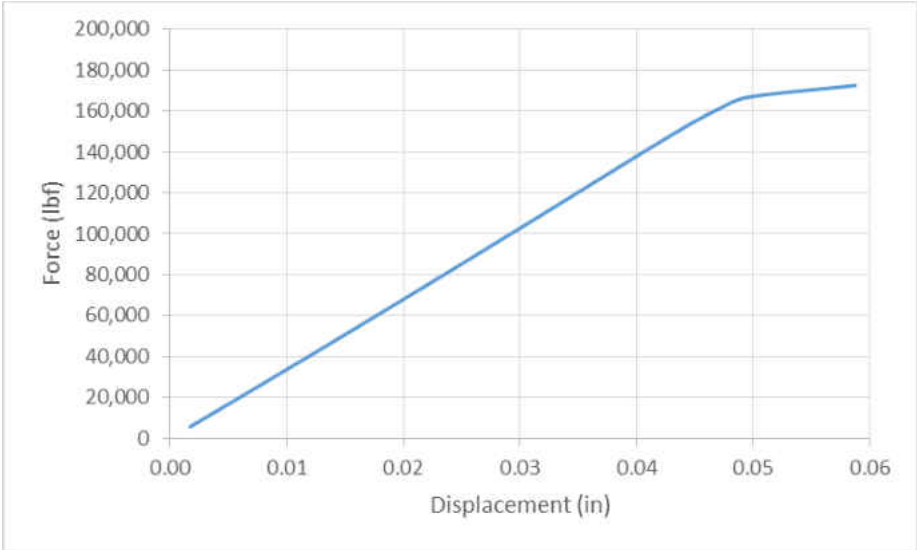


Figure 21: Load-Deflection Curve of Maximum Deflection Node for Model 7

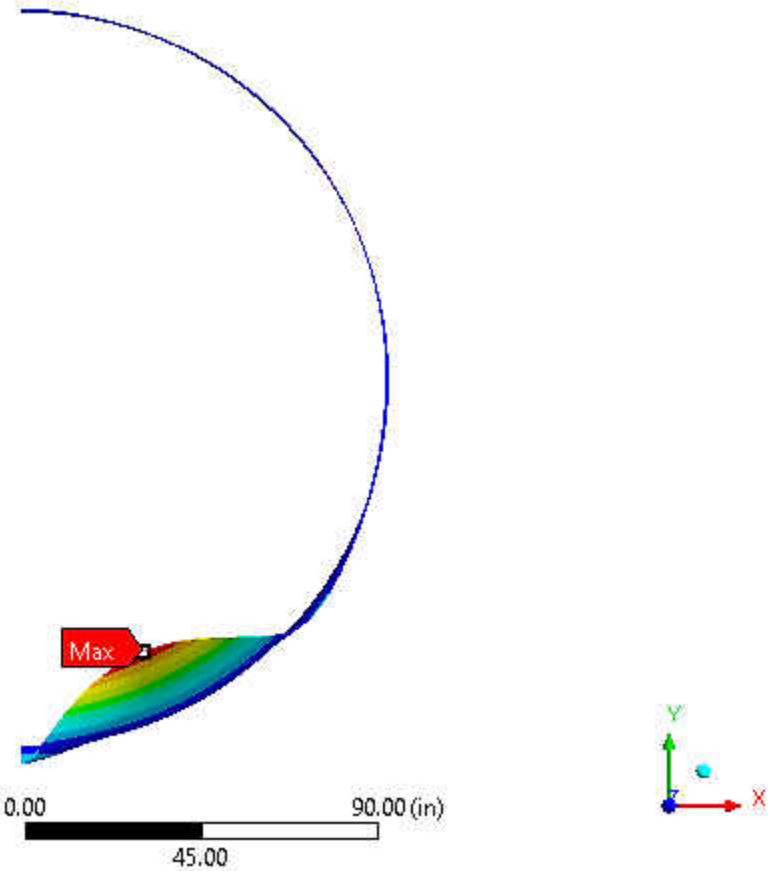


Figure 22: Post-Buckling Deflected Shape of Model 7

**Model 8**

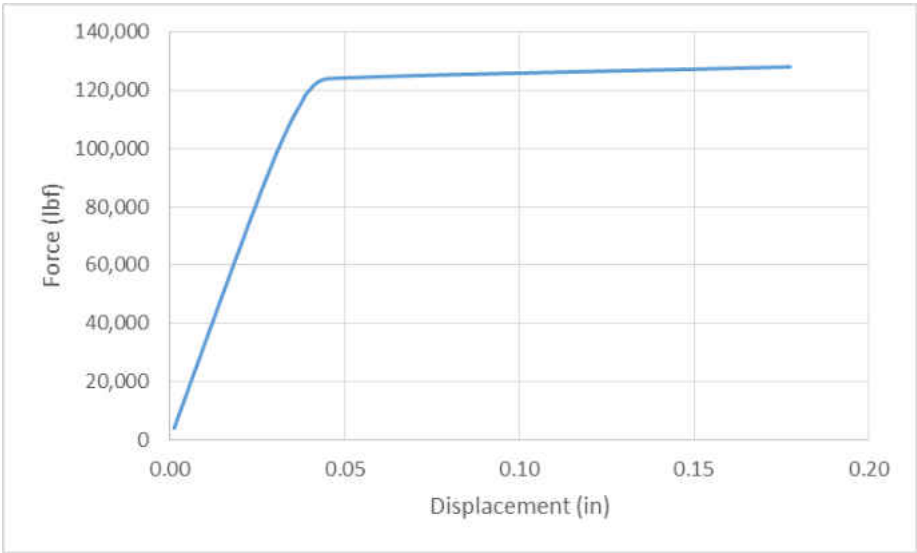


Figure 23: Load-Deflection Curve of Maximum Deflection Node for Model 8

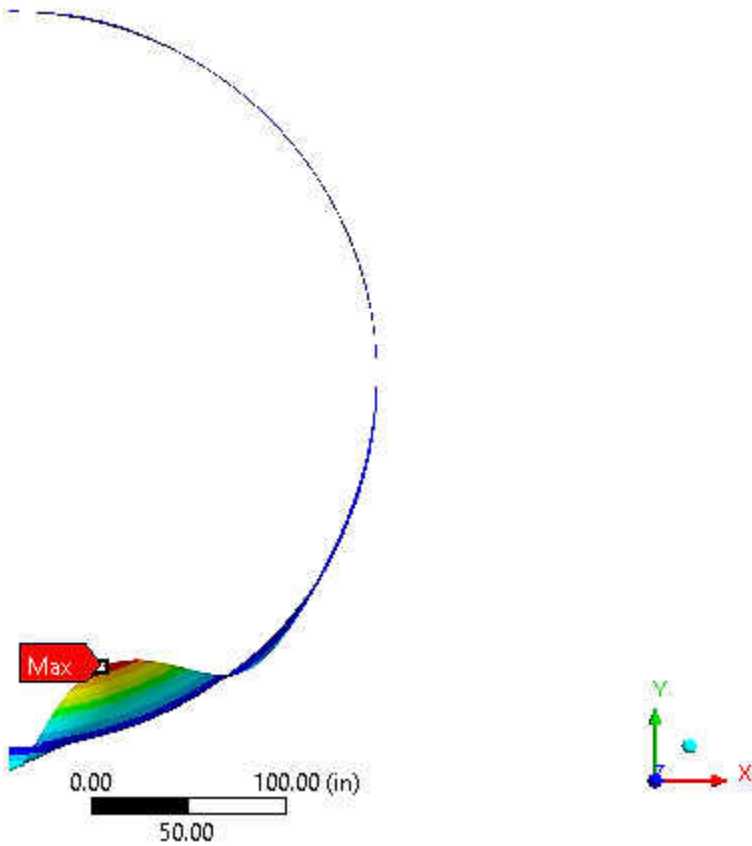


Figure 24: Post-Buckling Deflected Shape of Model 8

## Model 9

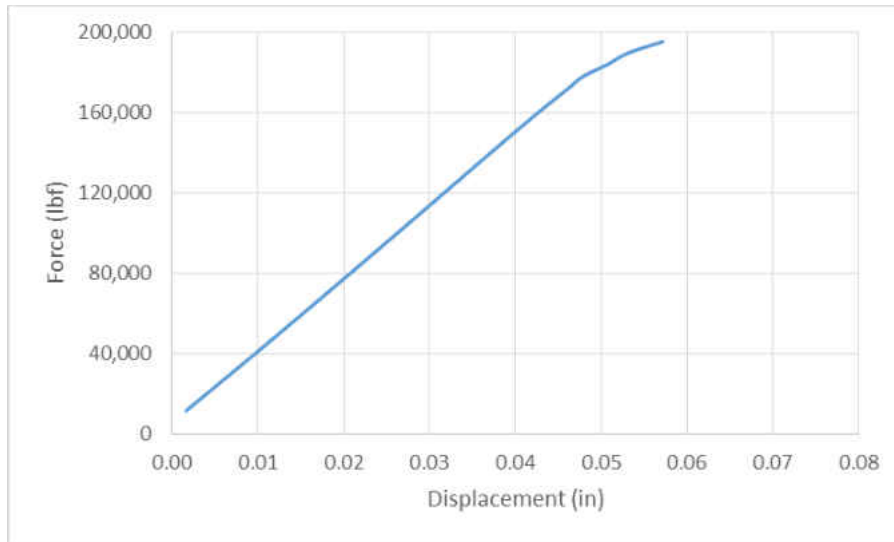


Figure 25: Load-Deflection Curve of Maximum Deflection Node for Model 9

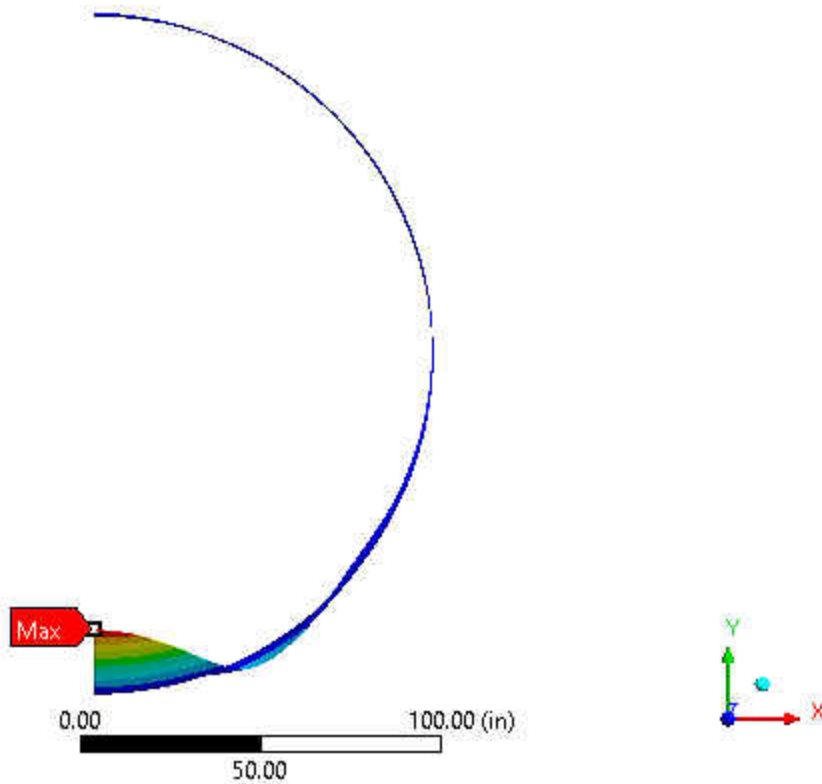


Figure 26: Post-Buckling Deflected Shape of Model 9

**Model 10**

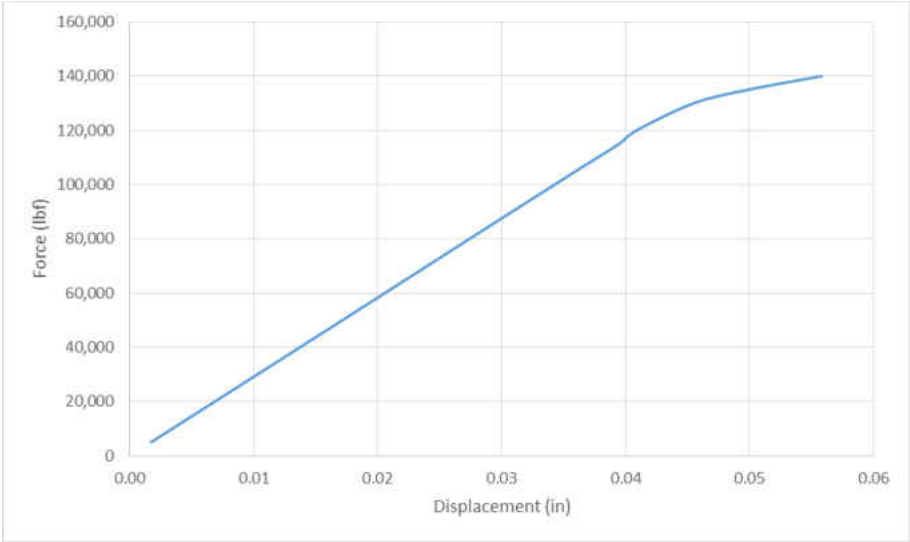


Figure 27: Load-Deflection Curve of Maximum Deflection Node for Model 10

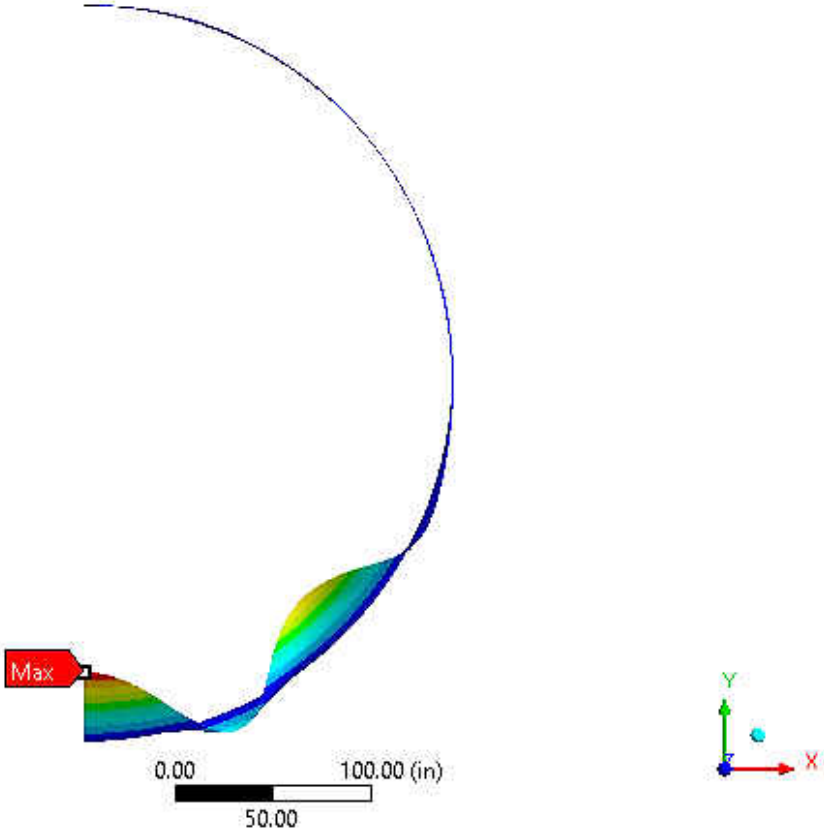


Figure 28: Post-Buckling Deflected Shape of Model 10

**Model 11**

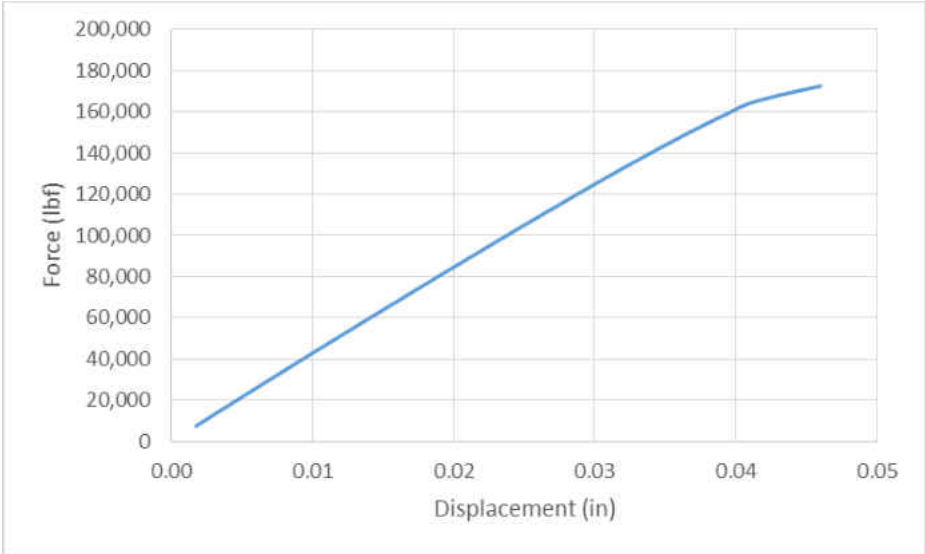


Figure 29: Load-Deflection Curve of Maximum Deflection Node for Model 11

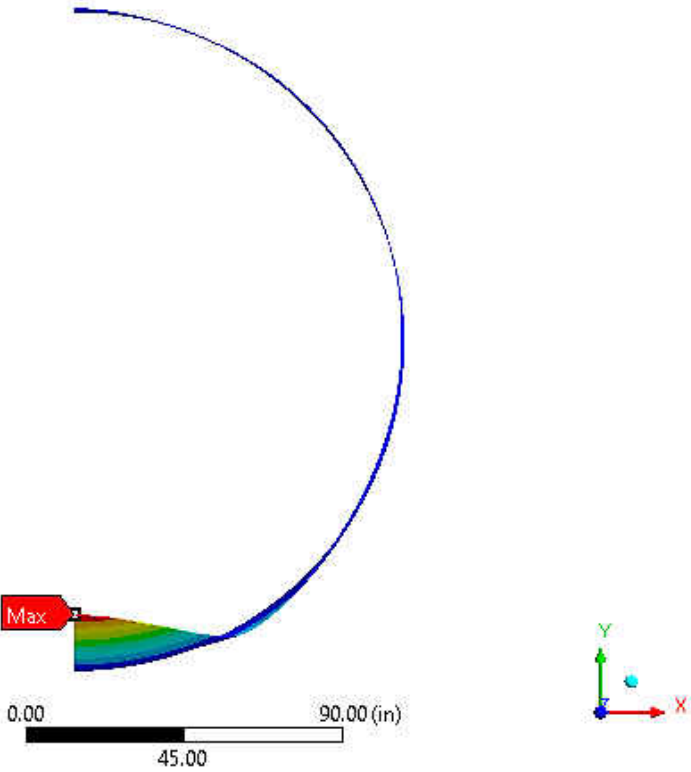


Figure 30: Post-Buckling Deflected Shape of Model 11



**Model 12**

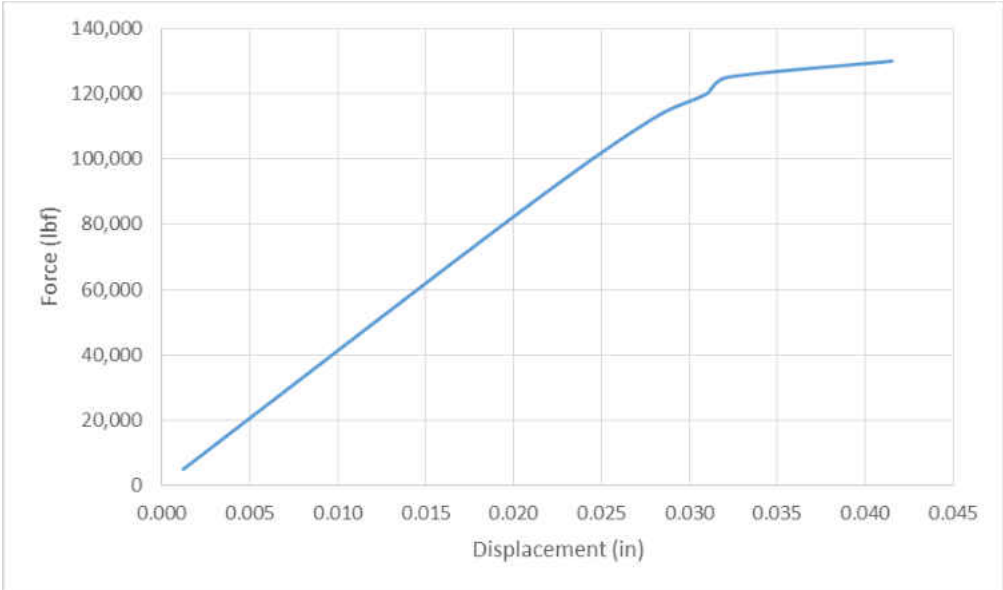


Figure 31: Load-Deflection Curve of Maximum Deflection Node for Model 12

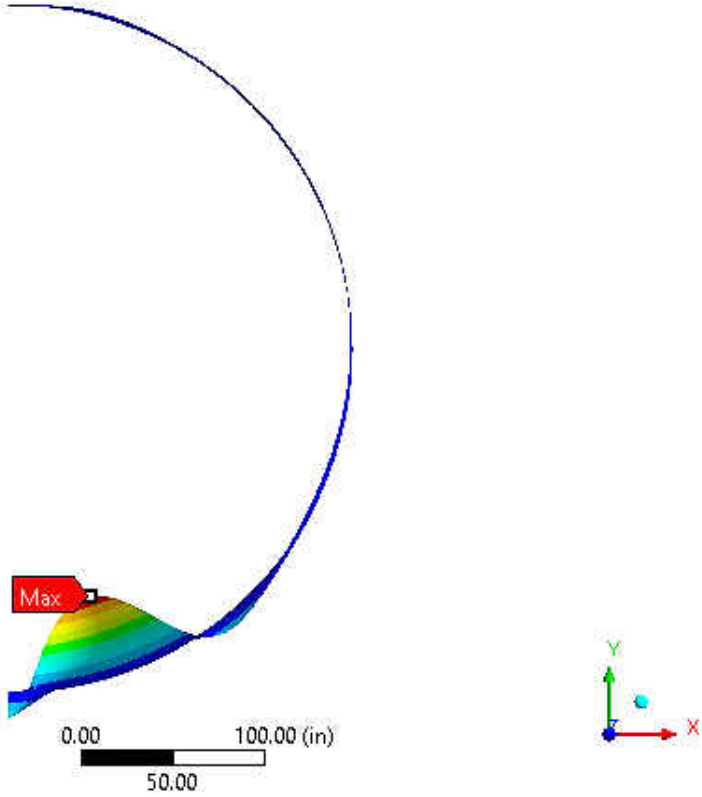


Figure 32: Post-Buckling Deflected Shape of Model 12

## CHAPTER V: MODAL ANALYSIS

Modal analysis on ANSYS is used to determine the vibration characteristics, by calculating the natural frequencies and mode shapes of the models created. Modal analysis was used in order to determine the mass coefficients for the Rayleigh damping method. External forces and damping are not considered in modal analysis, due to the structure being in free vibration.

Equation 3 is the equation of motion for an undamped system, expressed in matrix notation.

$$[M]\{\ddot{u}\} + [K]\{u\} = \{0\} \quad (3)$$

Where:  $[M]$ : structural mass matrix  
 $[K]$ : structural stiffness matrix  
 $\{\ddot{u}\}$ : nodal acceleration vector  
 $\{u\}$ : nodal displacement vector

For a linear system, free vibrations will be harmonic of the form in Equation 4:

$$\{u\} = \{\phi_i\} \cos \omega_i t \quad (4)$$

Where:  $\{\phi_i\}$ : eigenvector representing the mode shape of the  $i^{\text{th}}$  natural frequency  
 $\omega_i$ :  $i^{\text{th}}$  natural angular frequency, rad/s  
 $t$ : time, seconds

For a free vibration analysis, Equation 5 is created by substituting Equation 4 into Equation 3.

$$(-\omega^2[M] + [K])\{\phi_i\} = \{0\} \quad (5)$$

If  $(-\omega^2[M] + [K])$  or  $\{\phi_i\}$  is equal to zero, then Equation 6 is satisfied. Since  $\{\phi_i\}=0$  is trivial, the mode shapes and natural frequency are determined only by  $[M]$  and  $[K]$  shown in Equation 6.

$$|[K] - \omega^2[M]| = 0 \quad (6)$$

In this case, ten values for natural frequencies were computed by ANSYS and the mode shapes were extracted for each cylindrical tank model. The natural frequencies computed in ANSYS must be converted to natural angular frequencies, for later use. This is done using Equation 7.

$$f = \frac{\omega}{2\pi} \quad (7)$$

Where:  $f$ : natural frequency, Hz  
 $\omega$ : natural angular frequency, rad/s

Table 5 displays the first natural frequency calculated by ANSYS for each of the twelve cylindrical tanks filled 90% with water. It was found that the natural frequencies decrease as D/t increases.

*Table 5: First Natural Frequencies for 90% Filled Tanks*

<b>Model</b>	<b>H/D</b>	<b>D/t</b>	<b>First Natural Frequencies (Hz)</b>
1	0.5	520.83	3.8775
2	0.5	1041.67	1.9381
3	0.75	520.83	3.0405
4	0.75	1041.67	1.5198
5	1	520.83	2.5882
6	1	1041.67	1.2926
7	1.25	520.83	2.3921
8	1.25	1041.67	1.1955
9	1.5	520.83	2.3147
10	1.5	1041.67	1.1583
11	2	520.83	2.0997
12	2	1041.67	1.0878

## Model 1

Table 6: Model 1 Natural Frequencies at 90% Filled

Mode	Natural Frequency (Hz)
1	3.8775
2	4.9601
3	5.0021
4	5.6304
5	5.7165
6	5.8131
7	6.5292
8	6.5668
9	6.7083
10	7.1548

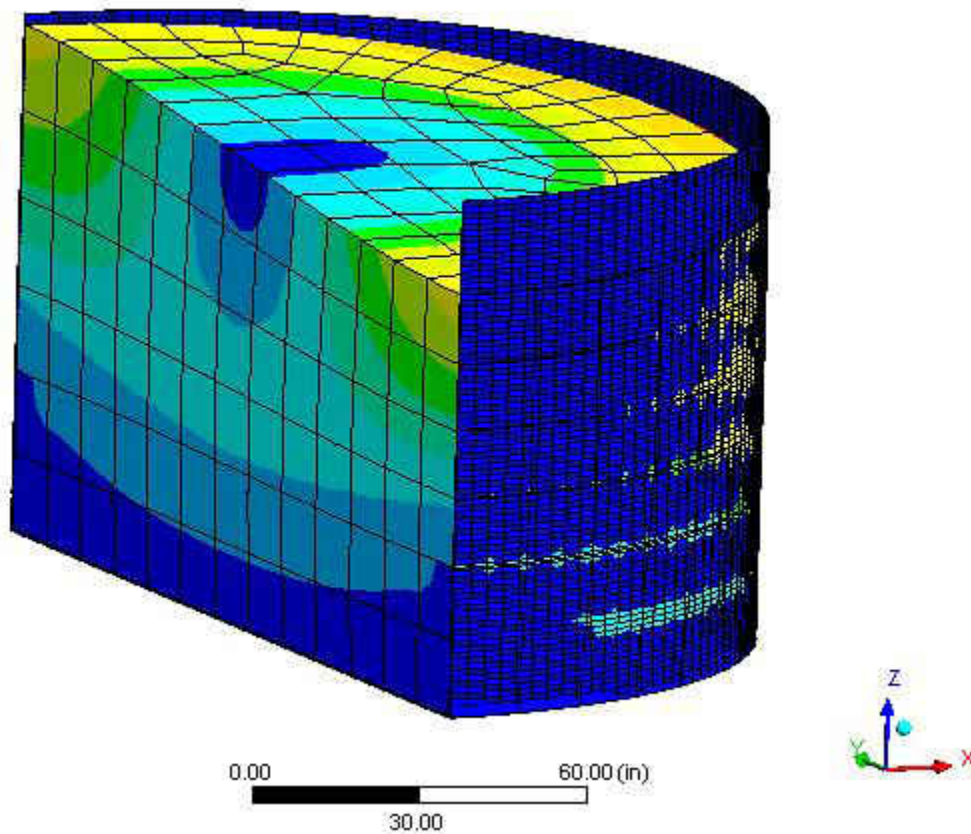


Figure 33: Model 1 First Mode 90% Filled (Scale 50:1)

## Model 2

Table 7: Model 2 Natural Frequencies at 90% Filled

Mode	Natural Frequency (Hz)
1	1.9381
2	2.4782
3	2.5036
4	2.8211
5	2.8594
6	2.9084
7	3.2183
8	3.2837
9	3.4136
10	3.6063

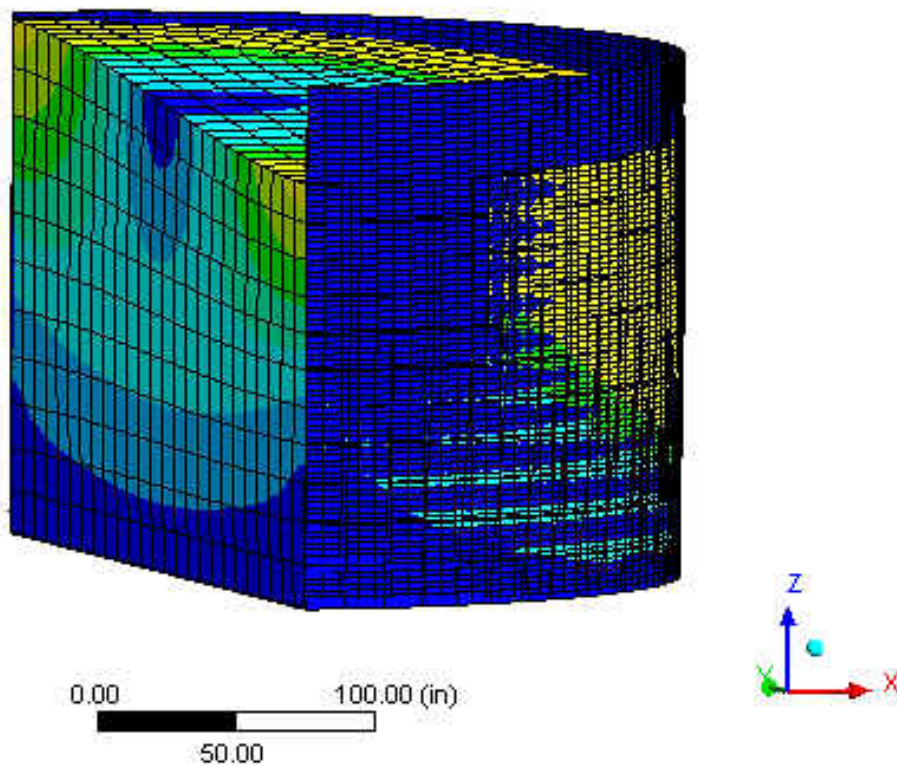


Figure 34: Model 2 First Mode 90% Filled (Scale 300:1)

### Model 3

Table 8: Model 3 Natural Frequencies at 90% Filled

Mode	Natural Frequency (Hz)
1	3.0405
2	3.8712
3	4.0707
4	4.4875
5	4.8952
6	5.0435
7	5.1735
8	5.8343
9	6.1937
10	6.2192

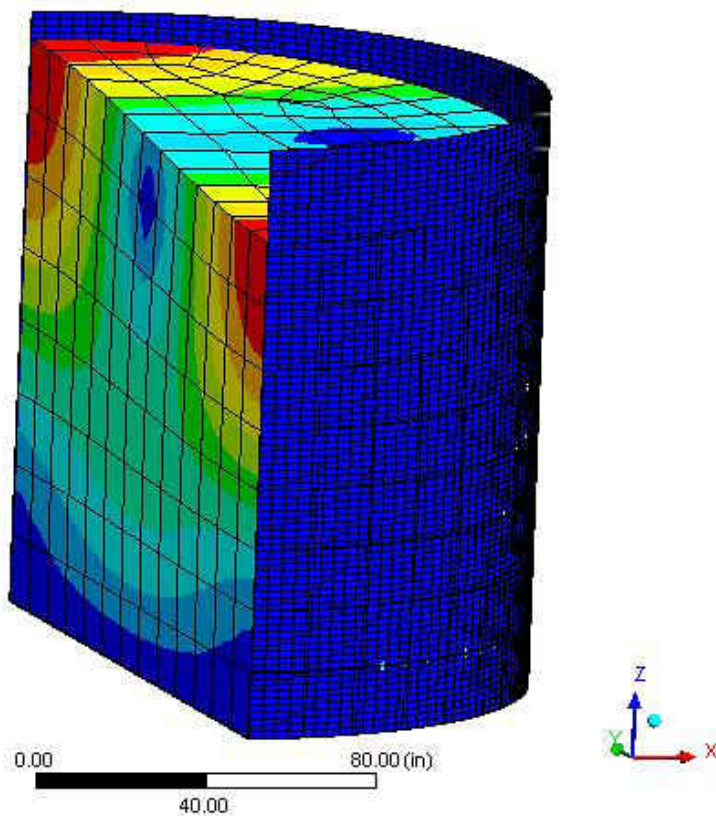


Figure 35: Model 3 First Mode 90% Filled (Scale 50:1)

## Model 4

Table 9: Model 4 Natural Frequencies at 90% Filled

Mode	Natural Frequency (Hz)
1	1.5198
2	1.9638
3	2.0513
4	2.2546
5	2.5163
6	2.5835
7	2.6715
8	2.9623
9	3.0918
10	3.0954

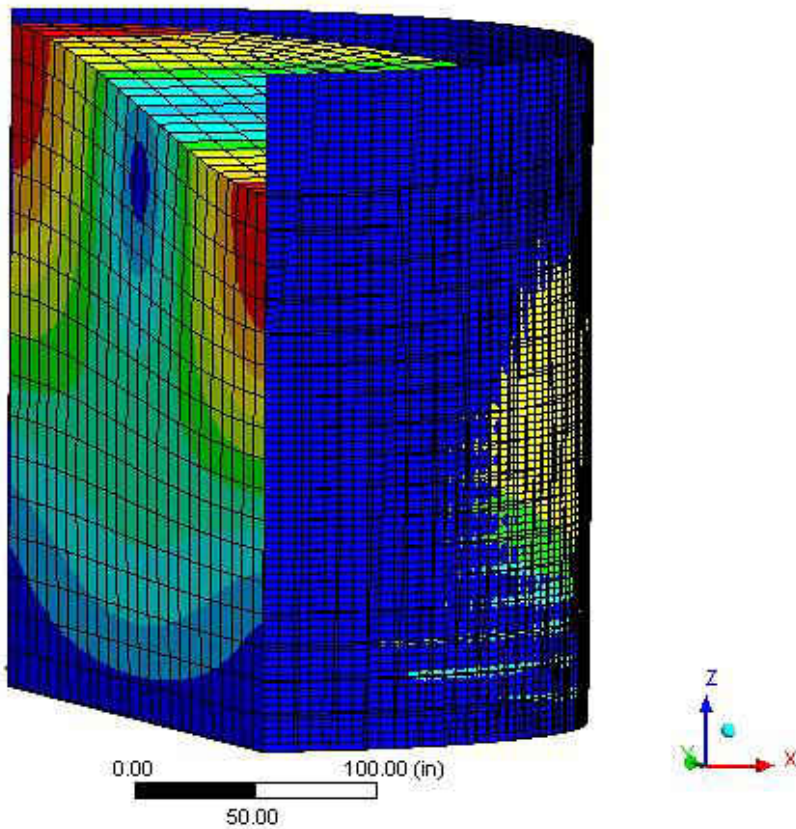


Figure 36: Model 4 First Mode 90% Filled (Scale 400:1)

## Model 5

Table 10: Model 5 Natural Frequencies at 90% Filled

Mode	Natural Frequency (Hz)
1	2.5882
2	3.2532
3	3.7246
4	4.2662
5	4.3029
6	4.7736
7	5.0344
8	5.3303
9	5.6095
10	5.6207

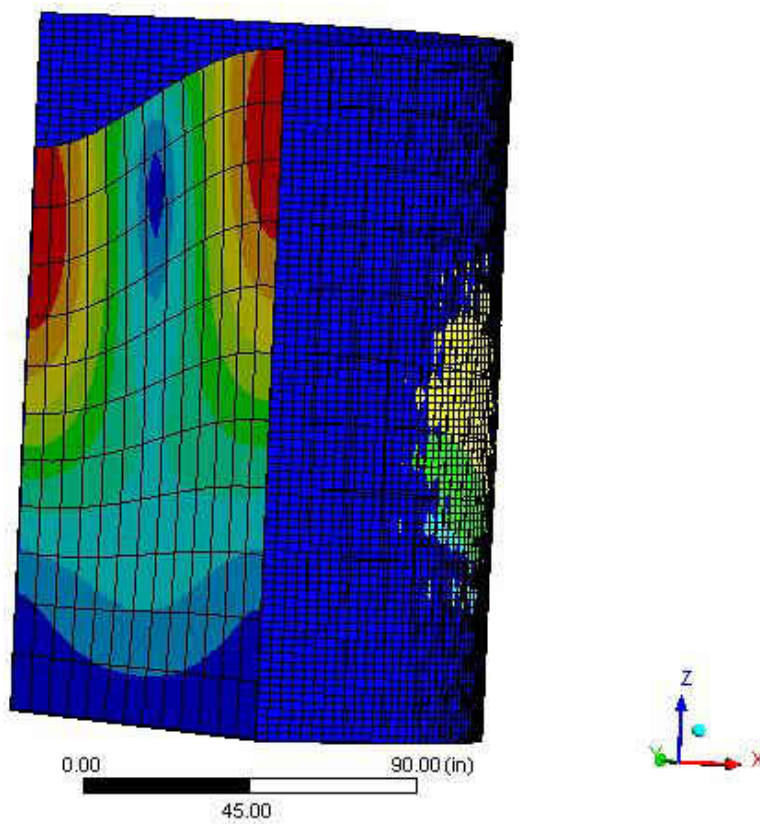


Figure 37: Model 5 First Mode 90% Filled (Scale 125:1)



## Model 6

Table 11: Model 6 Natural Frequencies at 90% Filled

Mode	Natural Frequency (Hz)
1	1.2926
2	1.6271
3	1.8937
4	2.1346
5	2.1994
6	2.4155
7	2.5141
8	2.6695
9	2.8101
10	2.8185

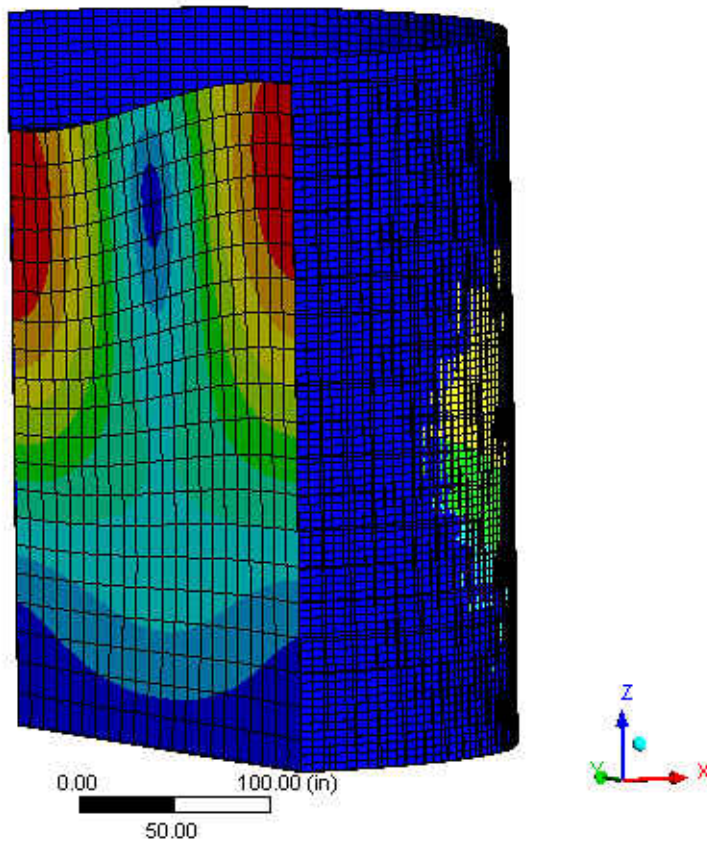


Figure 38: Model 6 First Mode 90% Filled (Scale 500:1)

## Model 7

Table 12: Model 7 Natural Frequencies at 90% Filled

Mode	Natural Frequency (Hz)
1	2.3921
2	2.856
3	3.4503
4	4.0451
5	4.0559
6	4.644
7	4.7362
8	4.8532
9	4.9925
10	5.0564

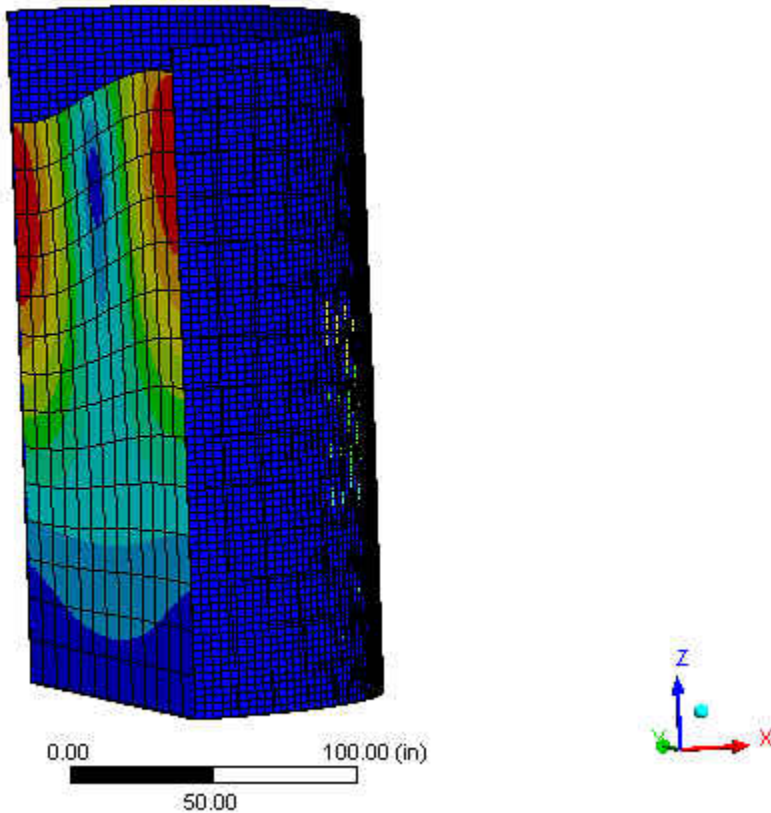


Figure 39: Model 7 First Mode 90% Filled (Scale 125:1)

## Model 8

Table 13: Model 8 Natural Frequencies at 90% Filled

Mode	Natural Frequency (Hz)
1	1.1955
2	1.3985
3	1.7386
4	2.0203
5	2.0267
6	2.3204
7	2.3822
8	2.4272
9	2.4977
10	2.5332

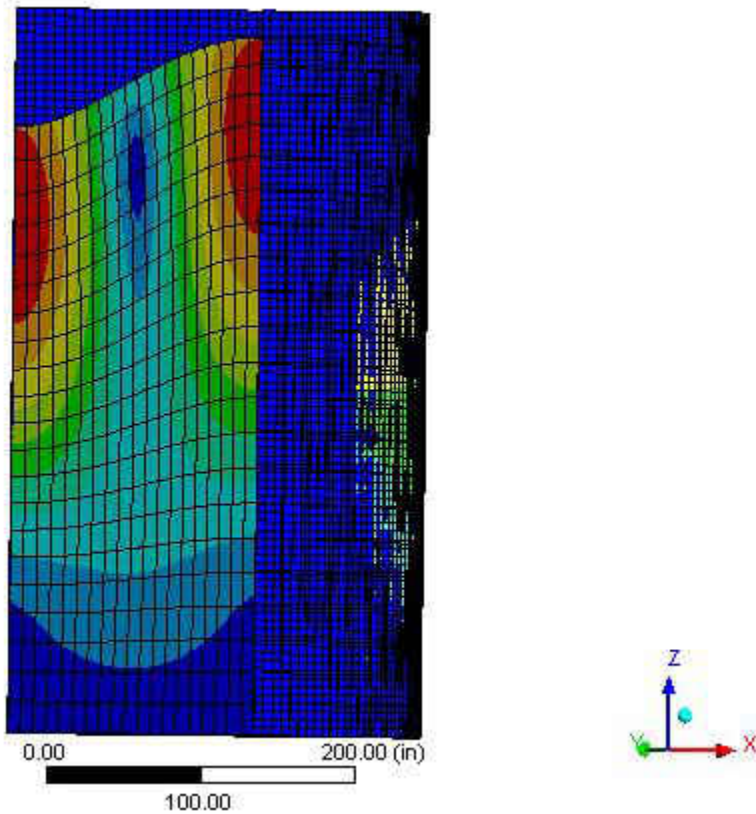


Figure 40: Model 8 First Mode 90% Filled (Scale 700:1)

## Model 9

Table 14: Model 9 Natural Frequencies at 90% Filled

Mode	Natural Frequency (Hz)
1	2.3147
2	2.6177
3	3.3332
4	3.7394
5	3.9735
6	4.1712
7	4.469
8	4.7275
9	4.7366
10	4.9811

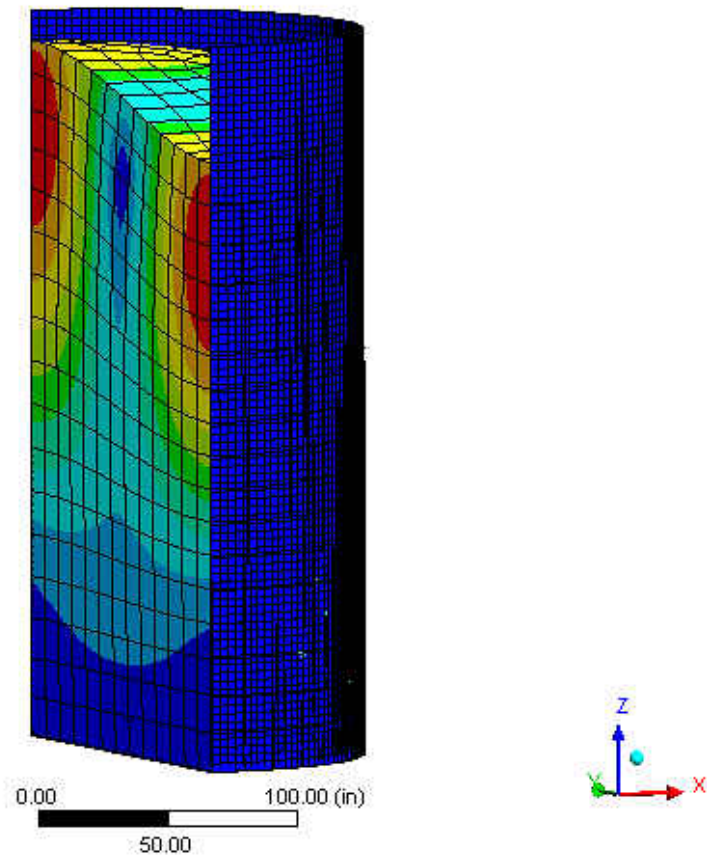


Figure 41: Model 9 First Mode 90% Filled (Scale 150:1)

## Model 10

Table 15: Model 10 Natural Frequencies at 90% Filled

Mode	Natural Frequency (Hz)
1	1.1583
2	1.3308
3	1.7353
4	1.8959
5	1.9941
6	2.0854
7	2.2385
8	2.37
9	2.3929
10	2.4899

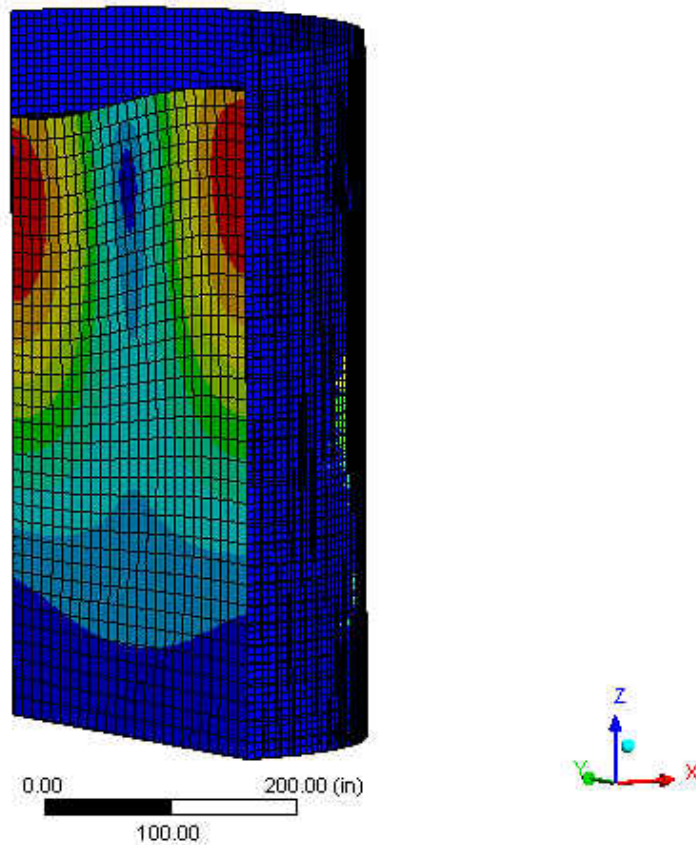


Figure 42: Model 10 First Mode 90% Filled (Scale 700:1)

## Model 11

Table 16: Model 11 Natural Frequencies at 90% Filled

Mode	Natural Frequency (Hz)
1	2.0997
2	2.291
3	3.0599
4	3.1714
5	3.5519
6	3.9237
7	4.1659
8	4.4235
9	4.5614
10	4.7469

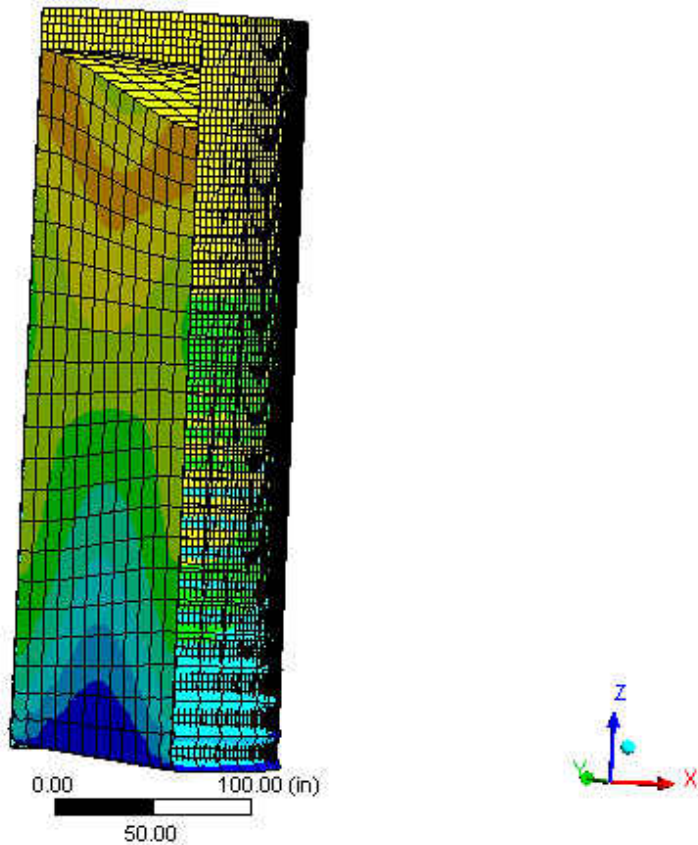


Figure 43: Model 11 First Mode 90% Filled (Scale 300:1)

## Model 12

Table 17: Model 12 Natural Frequencies at 90% Filled

Mode	Natural Frequency (Hz)
1	1.0878
2	1.1504
3	1.5442
4	1.6388
5	1.7774
6	1.9578
7	2.0817
8	2.2121
9	2.2792
10	2.3897

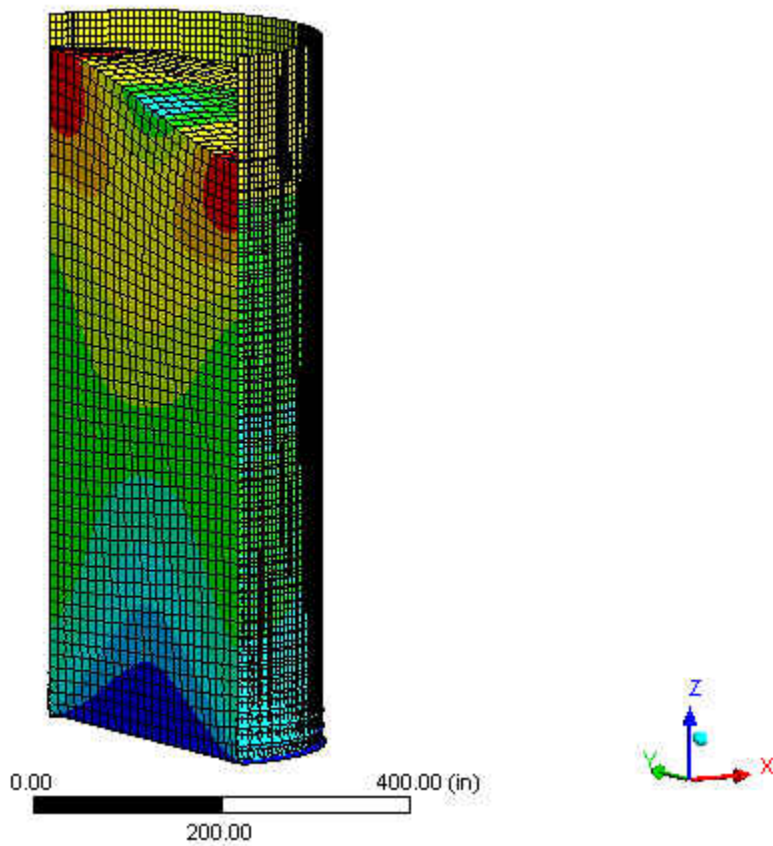


Figure 44: Model 12 First Mode 90% Filled (Scale 1500:1)

## CHAPTER VI: TRANSIENT DYNAMIC BUCKLING ANALYSIS

### 6.1 Definition and Method

Transient dynamic analysis is a method that considers inertia and damping effects and determines the dynamic response of a structure subjected to a time-dependent loading. The basic equation of motion, which is solved by a transient dynamic analysis is given in Equation 8.

$$[M]\{\ddot{u}\} + [C]\{\dot{u}\} + [K]\{u\} = \{F(t)\} \quad (8)$$

Where:

- [M]: mass matrix
- [C]: damping matrix
- [K]: stiffness matrix
- $\{\ddot{u}\}$ : nodal acceleration vector
- $\{\dot{u}\}$ : nodal velocity vector
- $\{u\}$ : nodal displacement vector
- $\{F(t)\}$ : load vector

Transient dynamic analysis was used to determine the dynamic buckling loads for the cylindrical tanks. The twelve cylindrical tanks were modeled with half symmetry and fixed-free support. Each tank was filled to 90% of the height, in order to determine the buckling loads for the fluid-filled cylindrical tank located in a region subjected to earthquakes. The cylindrical tanks were subjected to the acceleration of the El Centro earthquake. Large deformations and elastoplastic stress-strain properties were assumed for each model and the bilinear isotropic hardening was included with a yield stress of 50,000 psi (344.74 MPa) and a tangent modulus of 2,000,000 psi (13,789.51 MPa). Budiansky and Roth criterion, which states that the dynamic



buckling occurs when a small increase in the loading will cause a large increase in displacement, was used to find the buckling loads for the twelve cylindrical tanks.

The damping method that is used in the computer program ANSYS is the Rayleigh damping method. For this analysis, the damping is assumed as Rayleigh mass proportional damping given in Equation 9 (Djermane et al. 2014).

$$[C] = a_0[M] \quad (9)$$

Where:  $a_0$ : damping coefficient, using the mode's natural frequency

The damping coefficient is calculated using Equation 10.

$$a_0 = 2\omega_n\zeta_n \quad (10)$$

Where:  $\omega_n$ : natural angular frequencies, rad/s

$\zeta_n$ : critical damping ratio, generally between 2% and 3%

For this project, the critical damping ratio was set to 2%. The damping coefficients were calculated and were input into the ANSYS transient analysis models, indicating the damping coefficient for each cylindrical tank.

Sample calculation for the damping coefficients, using Model 1:

$$\omega = 2\pi * 3.8775 \text{ Hz} = 24.36 \text{ rad/s}$$

$$a_0 = 2 * 24.36 \frac{\text{rad}}{\text{s}} * 0.02 = 0.97452$$

The values computed for the mass coefficient of each cylindrical tank are displayed in Table 18.

Table 18: First Natural Frequencies and Mass Coefficients

Model	First Natural Frequencies (Hz)	Mass Coefficients ( $\alpha_0$ )
1	3.8775	0.97452
2	1.9381	0.48710
3	3.0405	0.76416
4	1.5198	0.38197
5	2.5882	0.65049
6	1.2926	0.32487
7	2.3921	0.60120
8	1.1955	0.30046
9	2.3147	0.58175
10	1.1583	0.29111
11	2.0997	0.52771
12	1.0878	0.27339

## 6.2 Earthquake Data

The earthquake data used for this study was the El Centro earthquake that occurred on May 18, 1940 in California. The earthquake data was found from the University of Berkley's National Information Service for Earthquake Engineering (University of Berkley 2016). Figure 45 is the first eight seconds of the accelerogram from the El Centro earthquake. That time interval was chosen, since the maximum amplitude for the earthquake occurred within the first eight seconds.

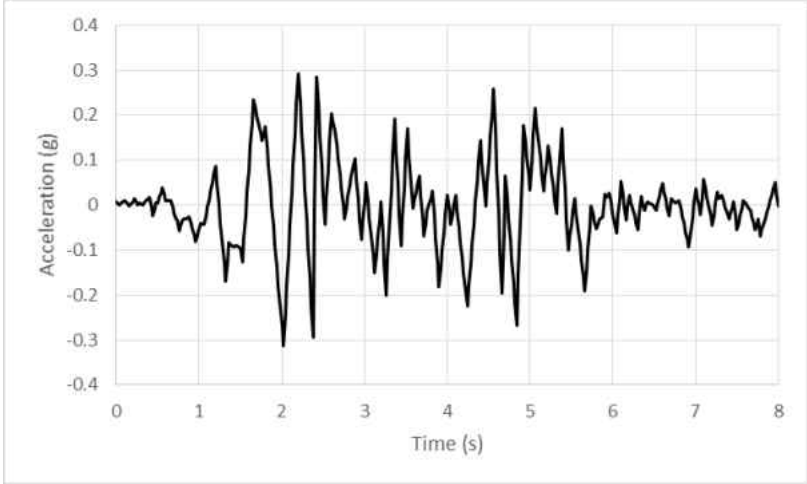


Figure 45: Accelerogram of the First Eight Seconds of the El Centro Earthquake

The effective earthquake force replaced the ground motion in this study, due to limitations within ANSYS Workbench. The El Centro earthquake acceleration, which had a peak ground acceleration (PGA) of 0.319g, was applied to every node of each of the cylindrical tank models.

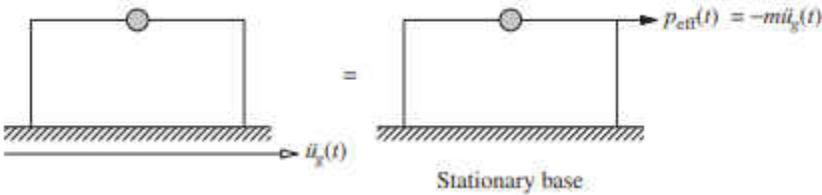


Figure 46: Effective Earthquake Force (Chopra 2012)

**6.3 Results**

Twelve cylindrical tanks were modeled and the El Centro earthquake was applied. Each model was filled with water at 90% of the height. The maximum displacements were plotted against the PGA level. The curves created from these simulations are pseudo equilibrium paths, which can determine the dynamic buckling capacity based on the transient displacements. Table

19 displays the results of the 90% filled cylindrical storage tanks subjected to the El Centro earthquake.

At the dynamic buckling loads, the von-Mises stresses were analyzed for each cylindrical tank model. Elastic buckling occurs if the models von-Mises stress is less than the yield stress and plastic buckling occurs when the von-Mises stress exceeds the yield stress. Model 8, Model 10, and Model 12 had a higher von-Mises stress than the yield stress of 50,000 psi (344.74 MPa). Model 8 had a von-Mises stress of 50,674 psi (349.38 MPa), Model 10 was 50,783 psi (350.14 MPa), and Model 12 was 51,889 psi (357.76 MPa).

*Table 19: Dynamic Buckling of the 90% Filled Cylindrical Tanks*

<b>H/D</b>	<b>PGA (g)</b>	
	<b>D/t=520.83</b>	<b>D/t=1,041.67</b>
0.5	4.25	1.75
0.75	2.98	1.71
1.0	2.70	1.22
1.25	2.22	1.2
1.5	2.04	0.84
2.0	1.99	0.8

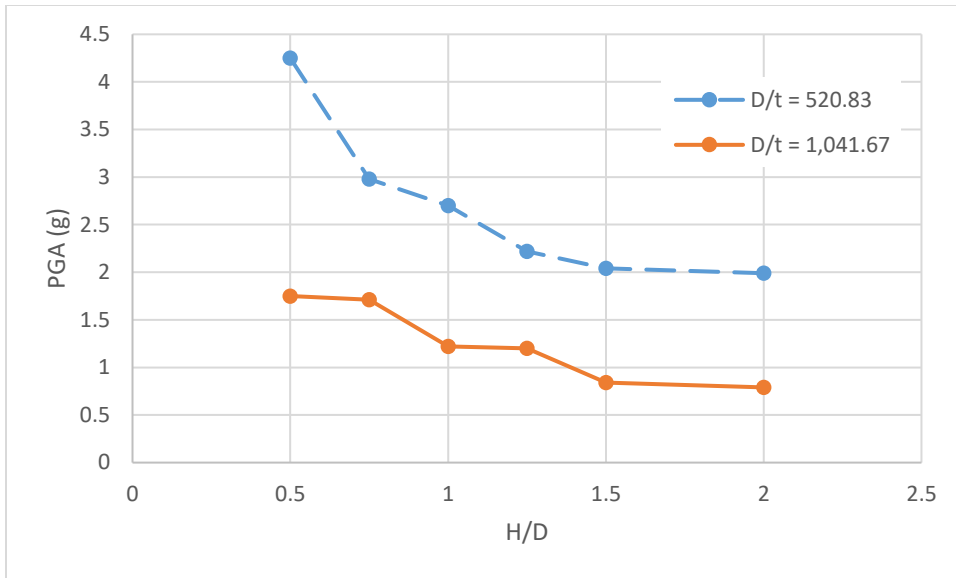


Figure 47: Dynamic Buckling Capacities from the Transient Analysis

Model 1

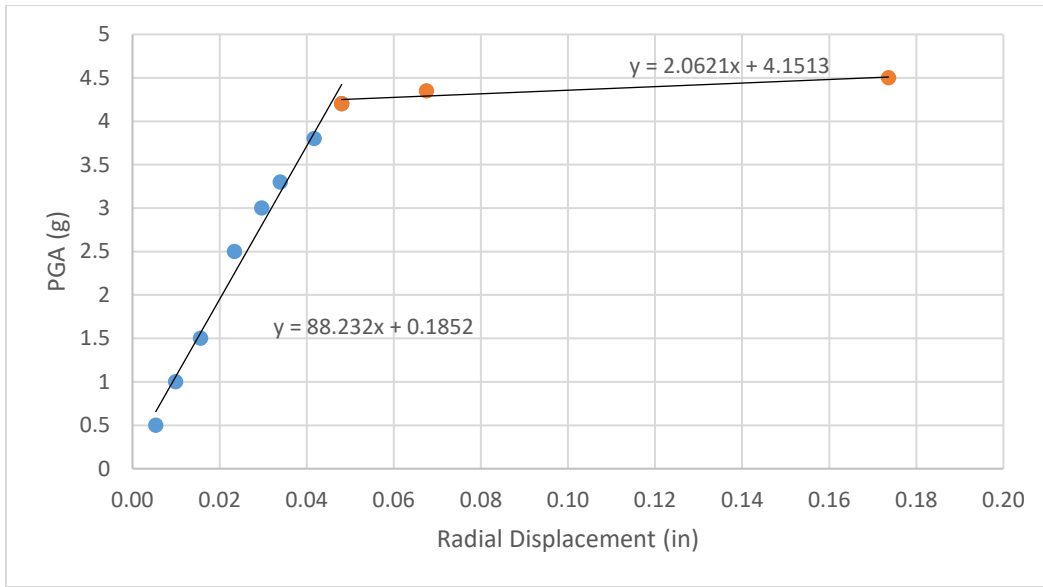


Figure 48: Pseudo Equilibrium Paths for the Critical Node of Model 1

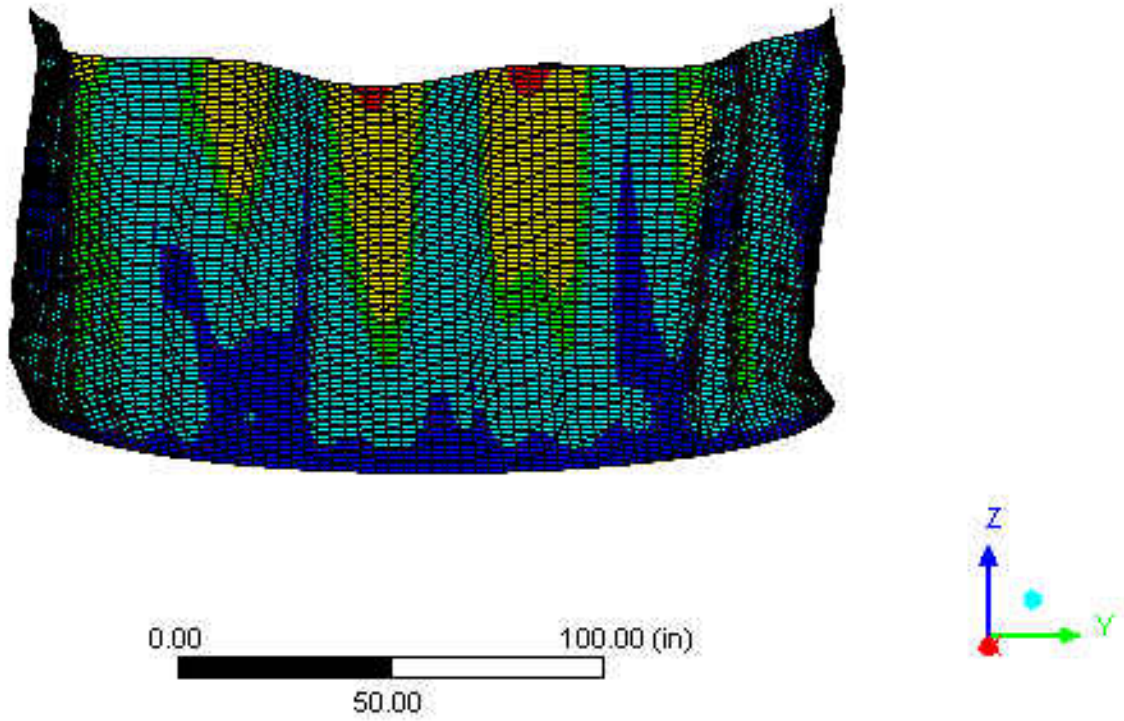


Figure 49: Shell Deformation of Model 1

## Model 2

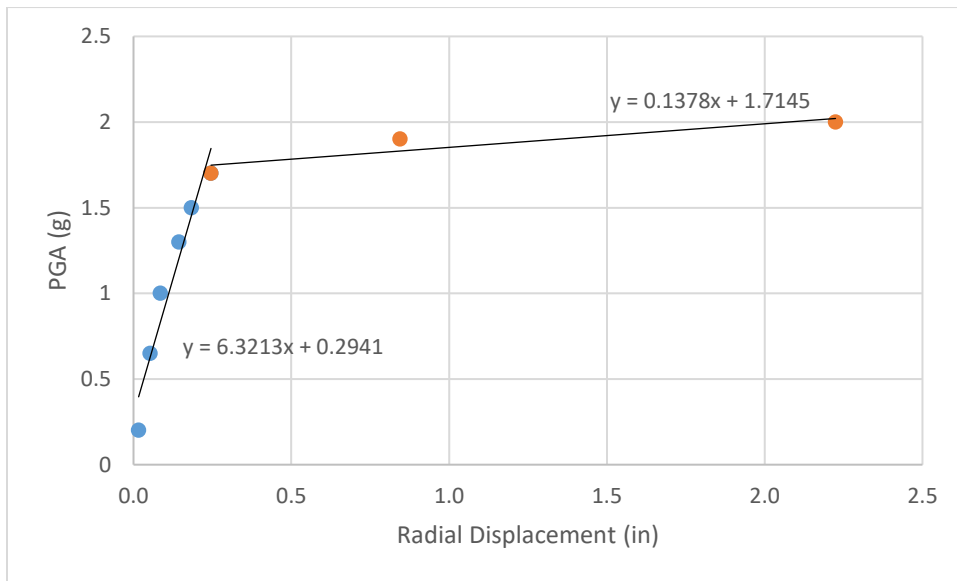


Figure 50: Pseudo Equilibrium Paths for the Critical Node of Model 2

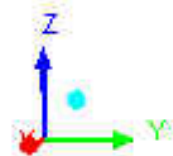
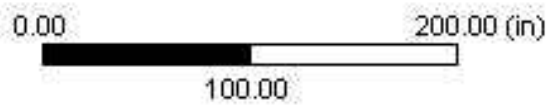
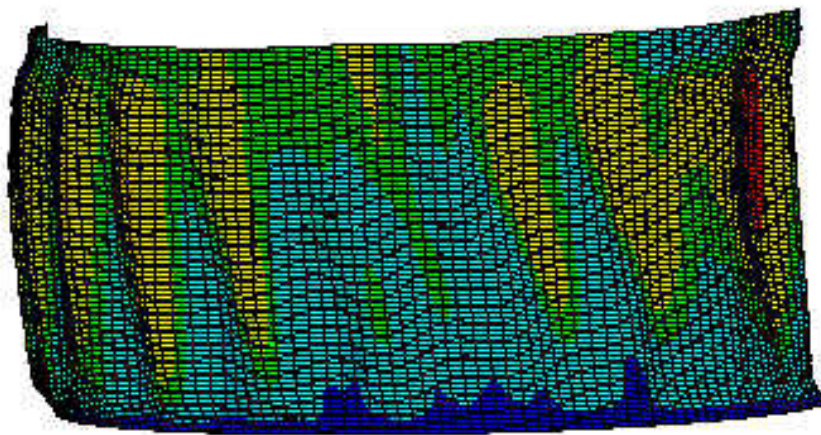


Figure 51: Shell Deformation of Model 2

### Model 3

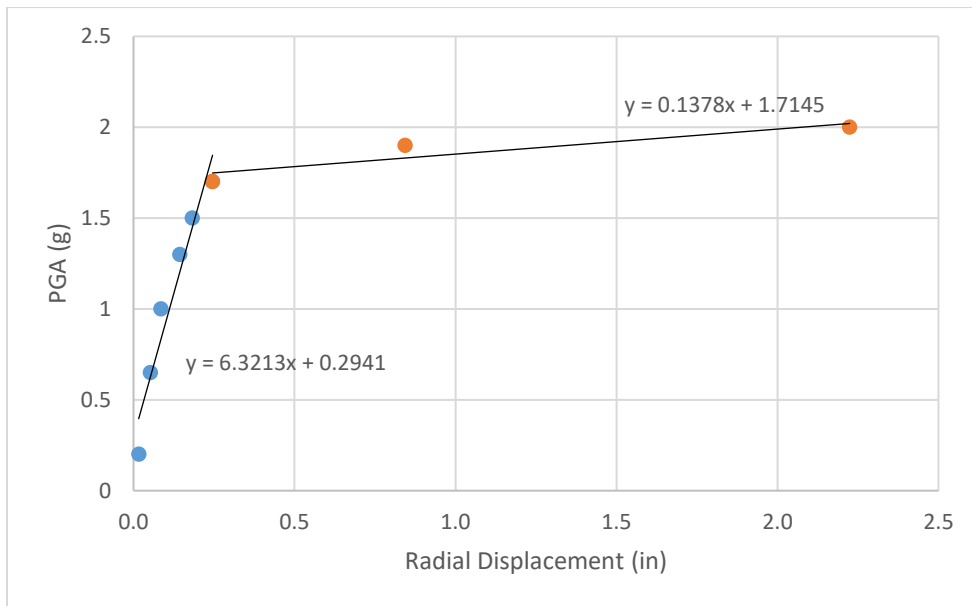


Figure 52: Pseudo Equilibrium Paths for the Critical Node of Model 3

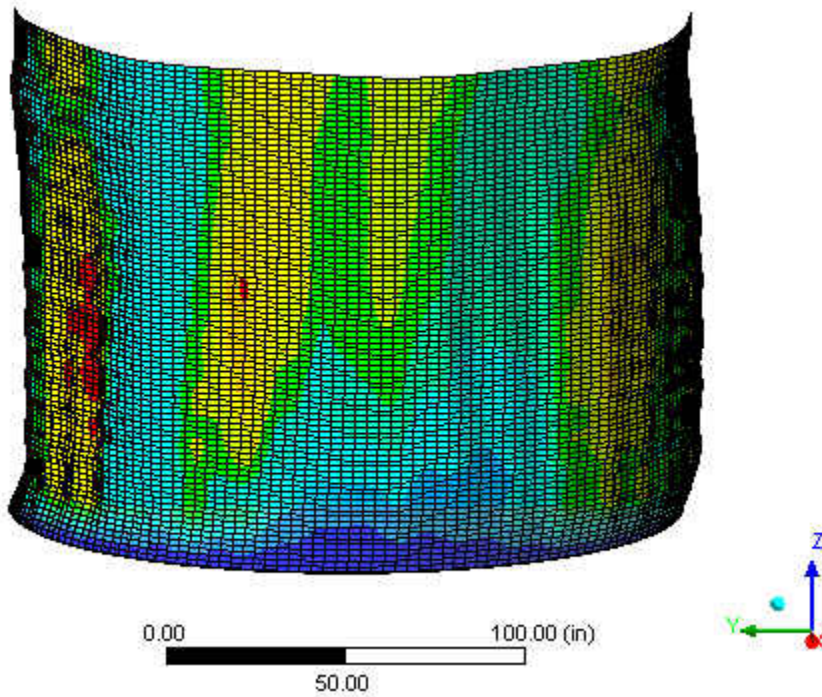


Figure 53: Shell Deformation of Model 3



# Model 4

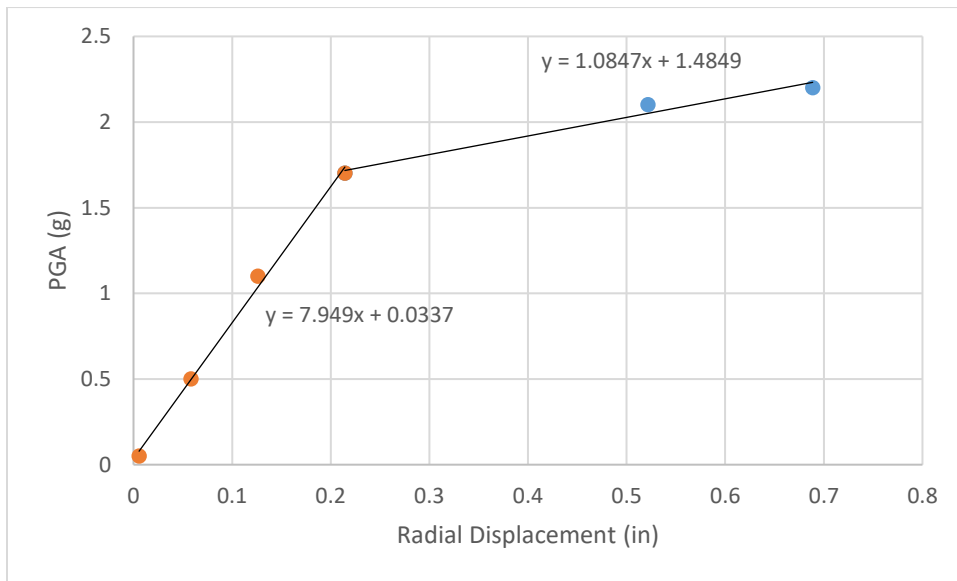


Figure 54: Pseudo Equilibrium Paths for the Critical Node of Model 4

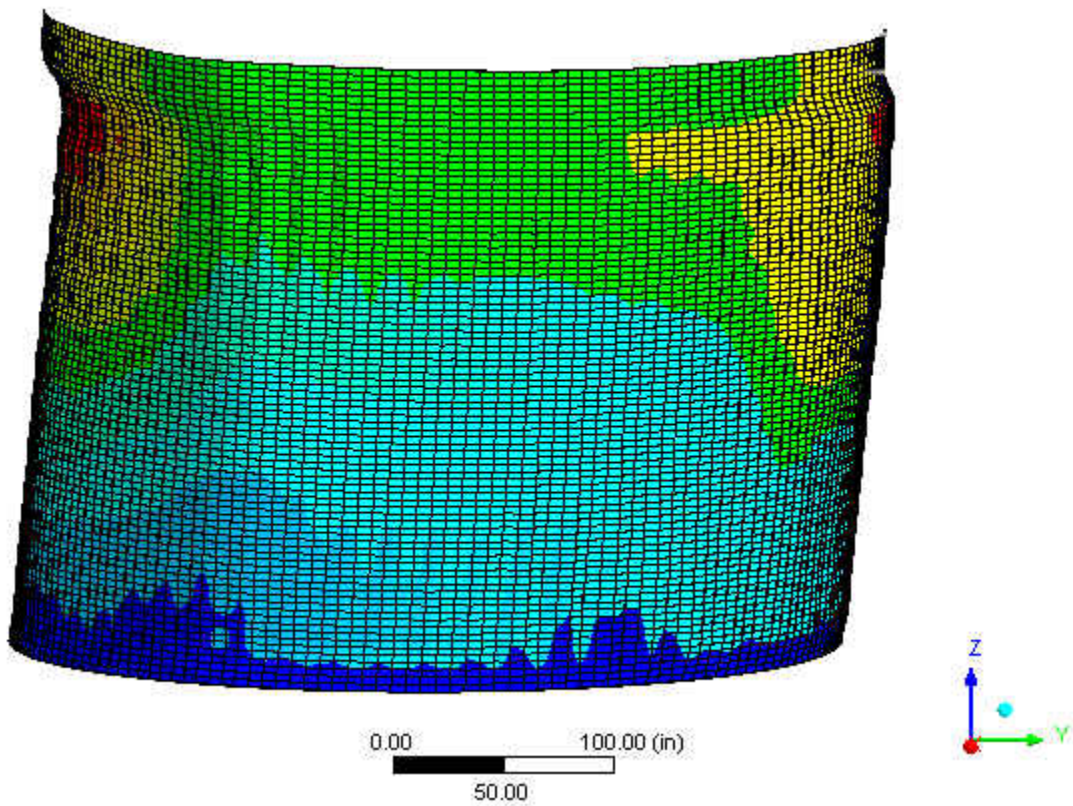


Figure 55: Shell Deformation of Model 4

## Model 5

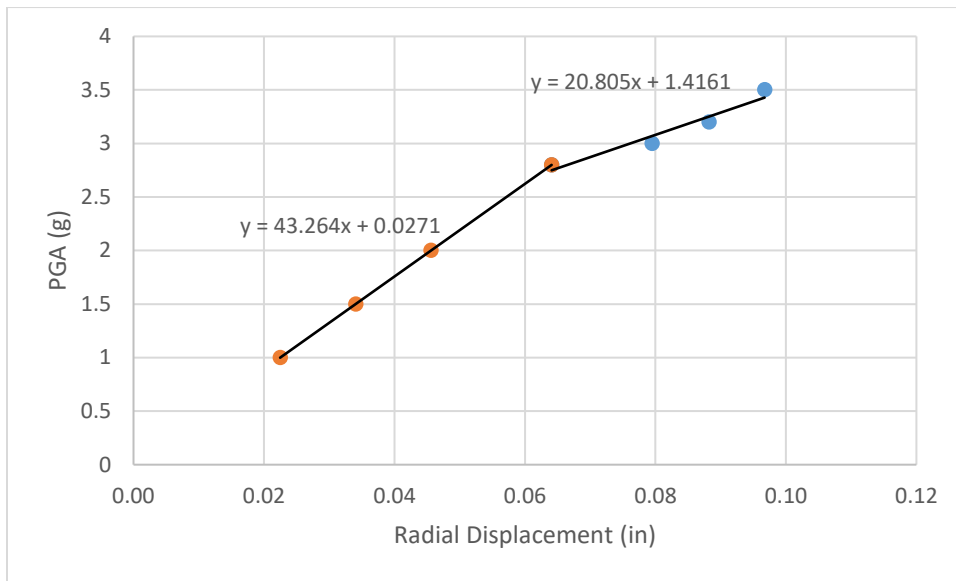


Figure 56: Pseudo Equilibrium Paths for the Critical Node of Model 5

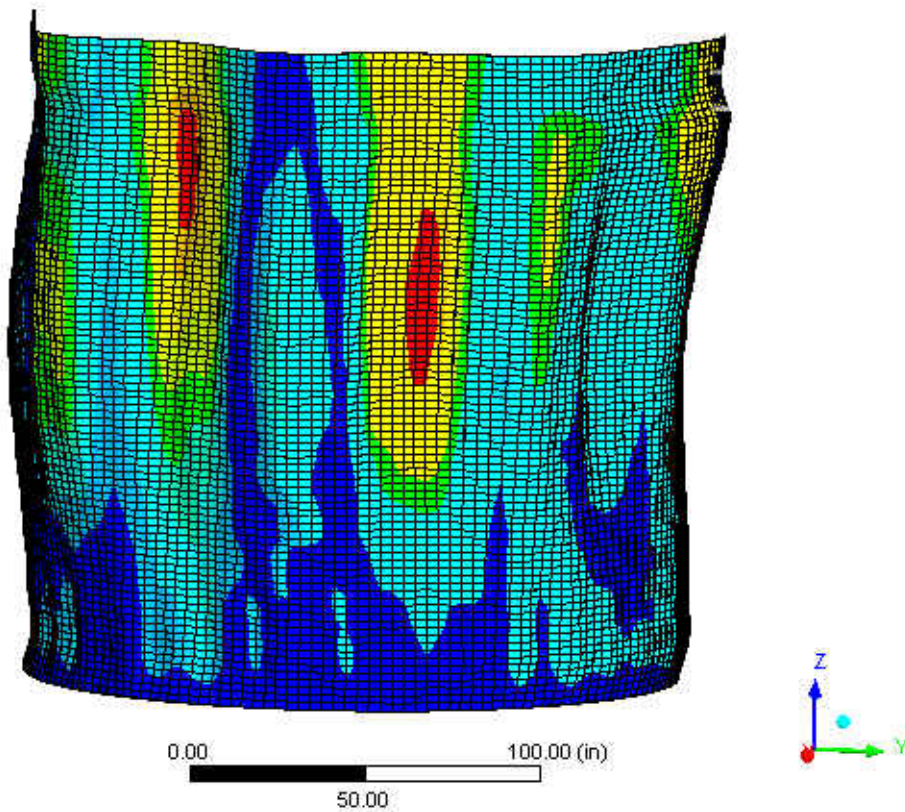


Figure 57: Shell Deformation of Model 5

# Model 6

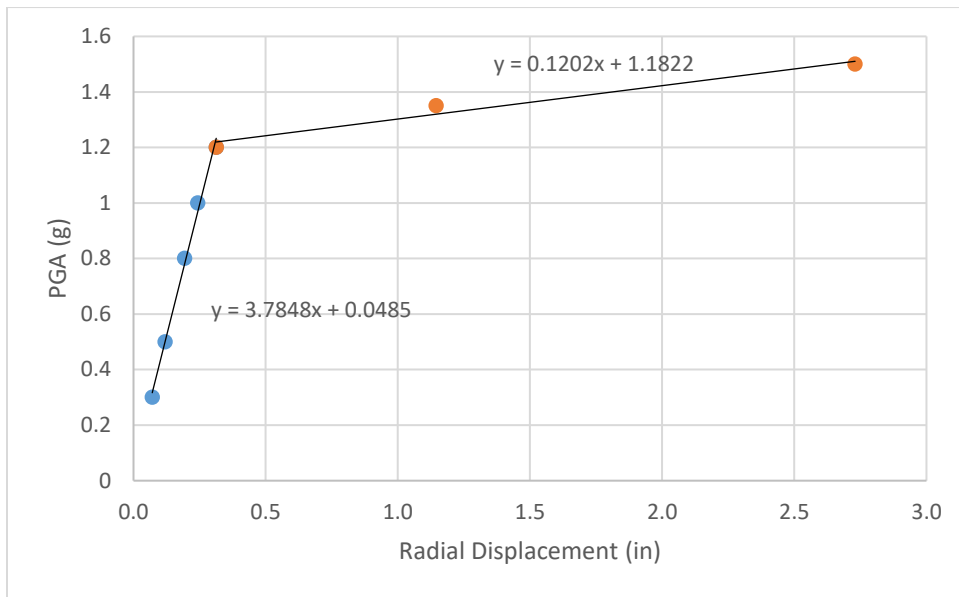


Figure 58: Pseudo Equilibrium Paths for the Critical Node of Model 6

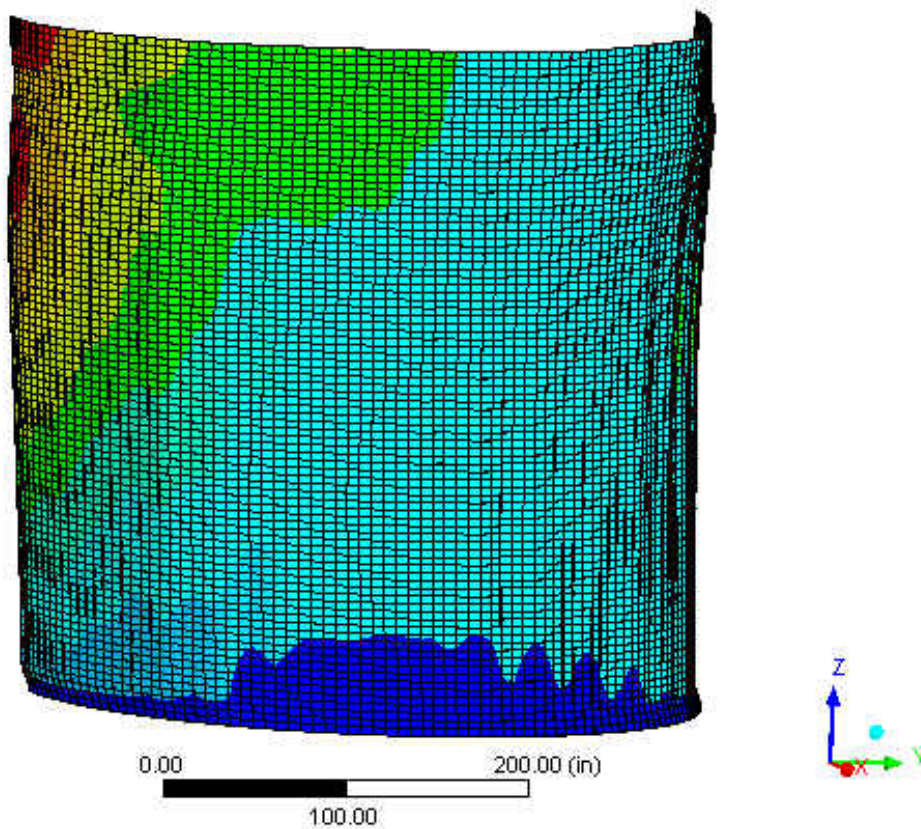


Figure 59: Shell Deformation of Model 6

Model 7

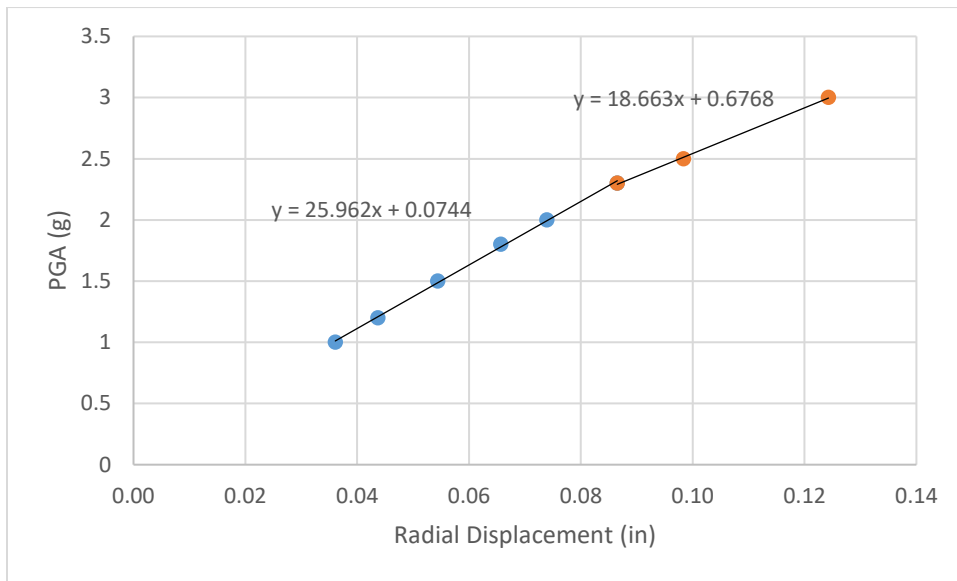


Figure 60: Pseudo Equilibrium Paths for the Critical Node of Model 7

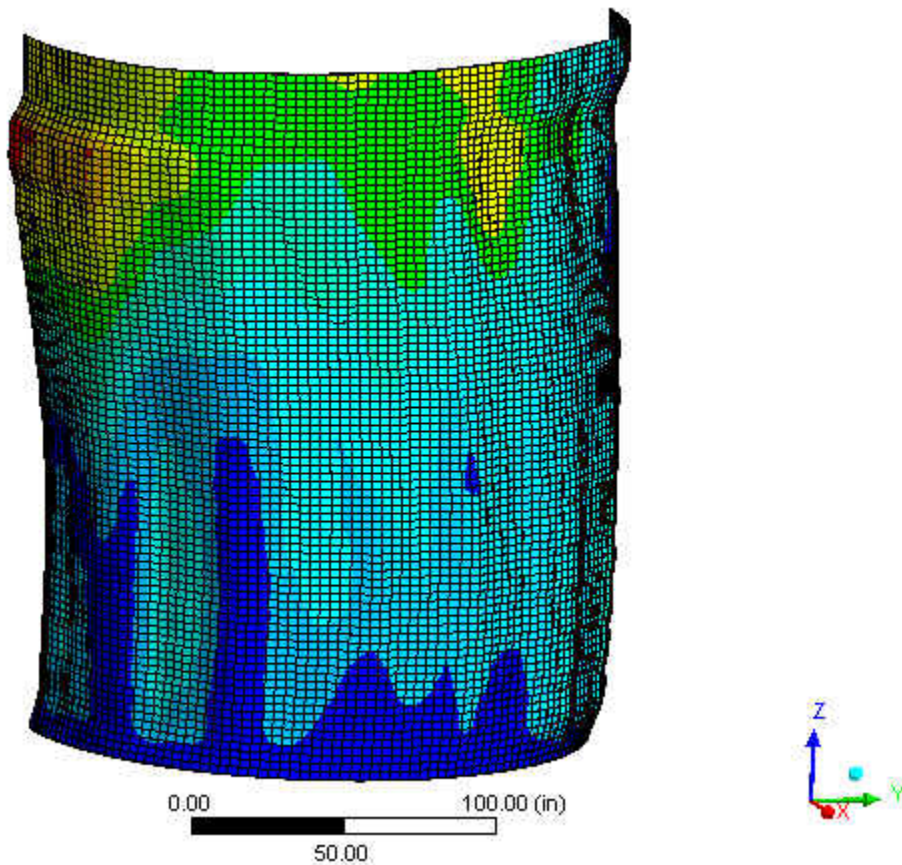


Figure 61: Shell Deformation of Model 7

# Model 8

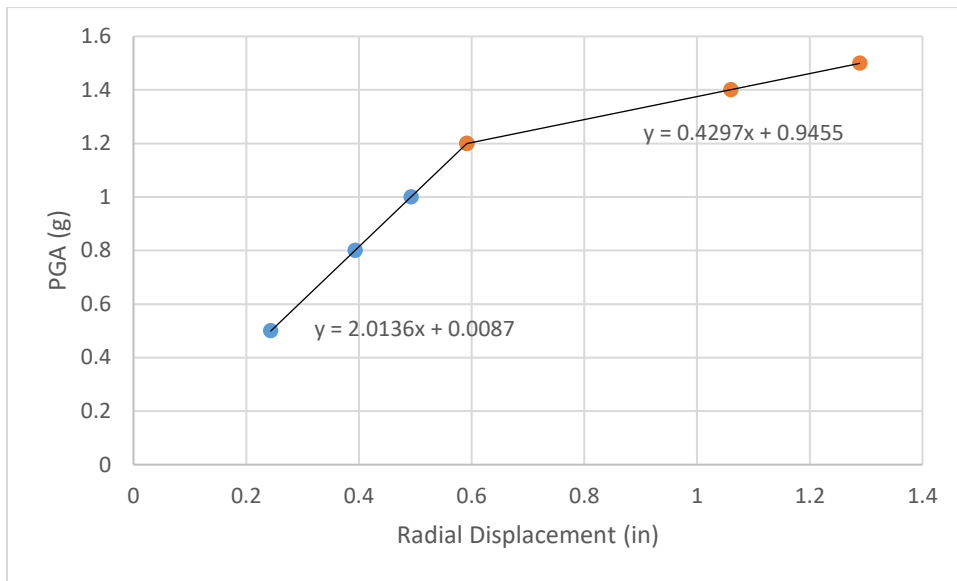


Figure 62: Pseudo Equilibrium Paths for the Critical Node of Model 8

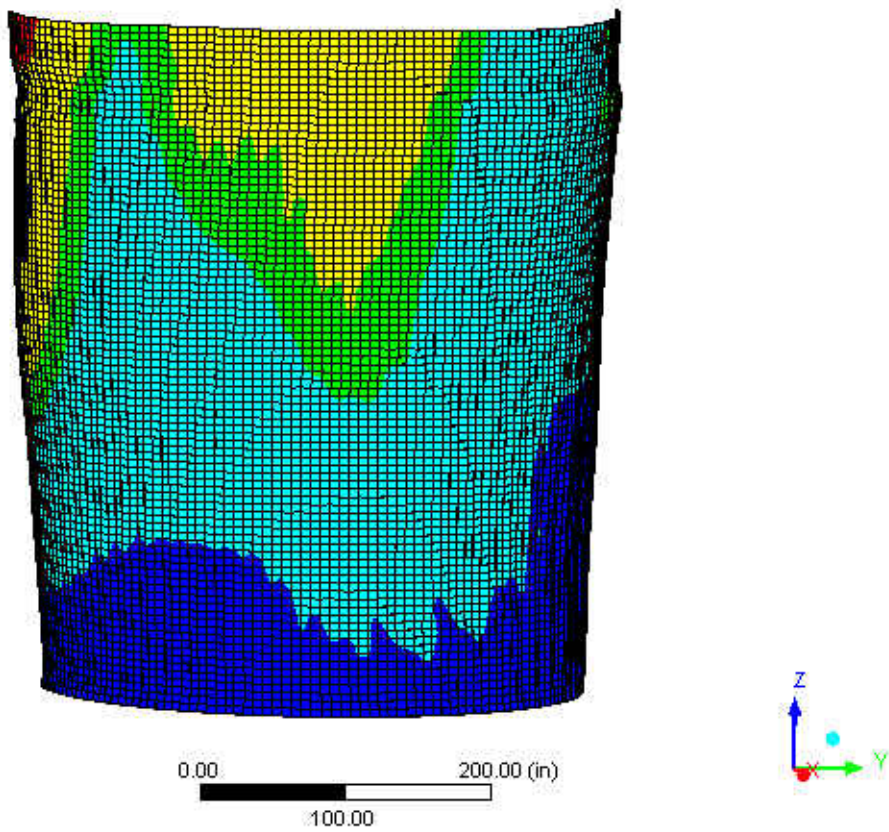


Figure 63: Shell Deformation of Model 8

# Model 9

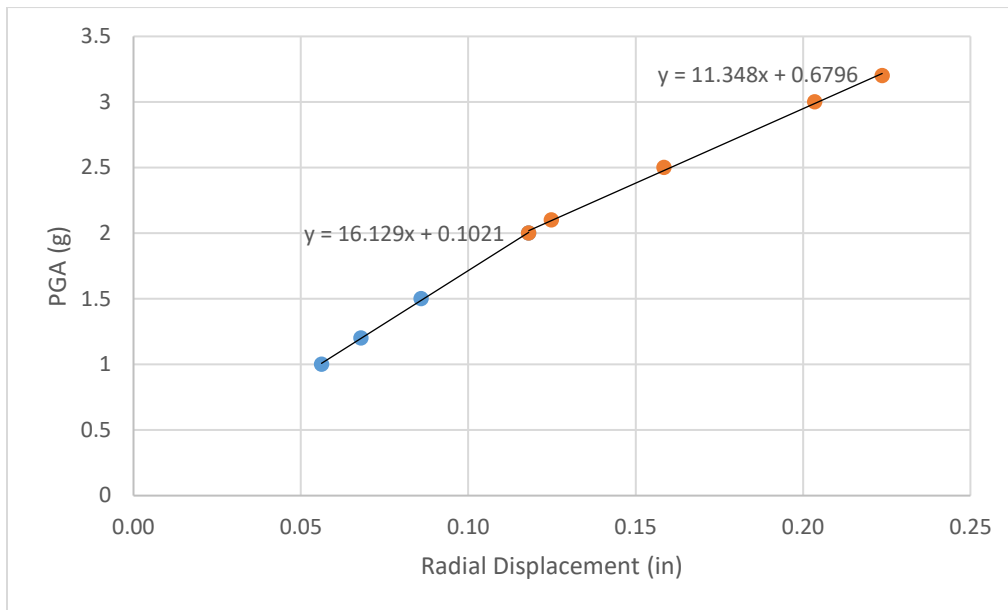


Figure 64: Pseudo Equilibrium Paths for the Critical Node of Model 9

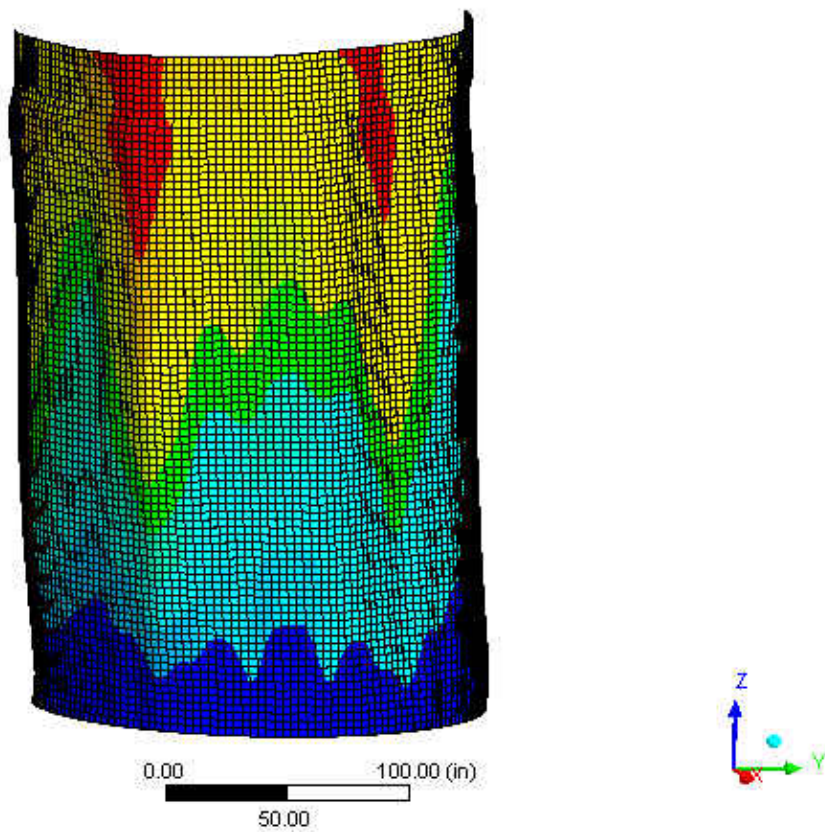


Figure 65: Shell Deformation of Model 9

# Model 10

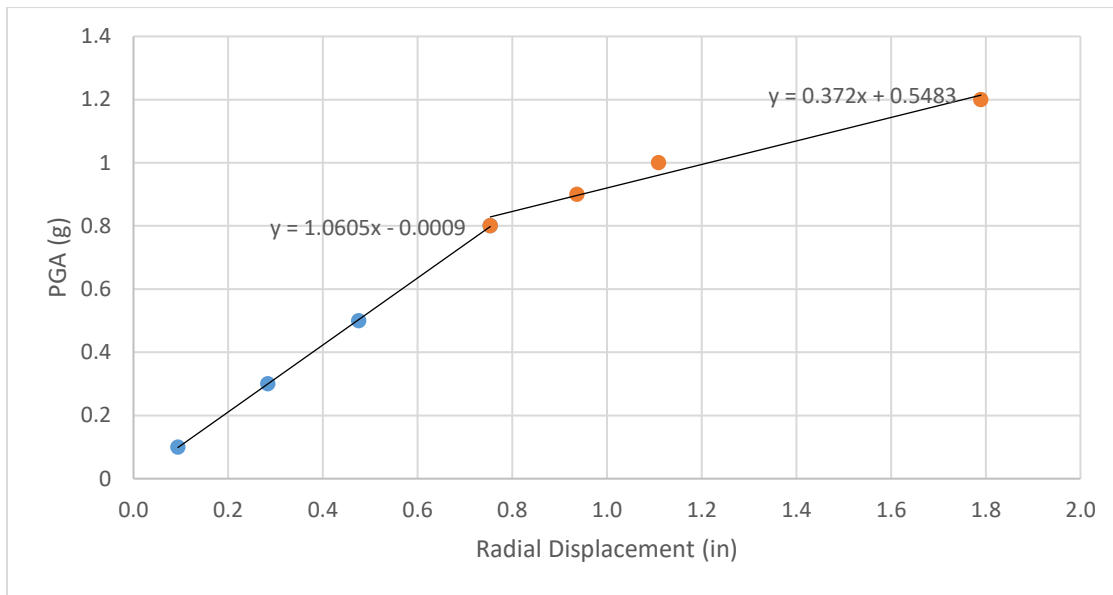


Figure 66: Pseudo Equilibrium Paths for the Critical Node of Model 10

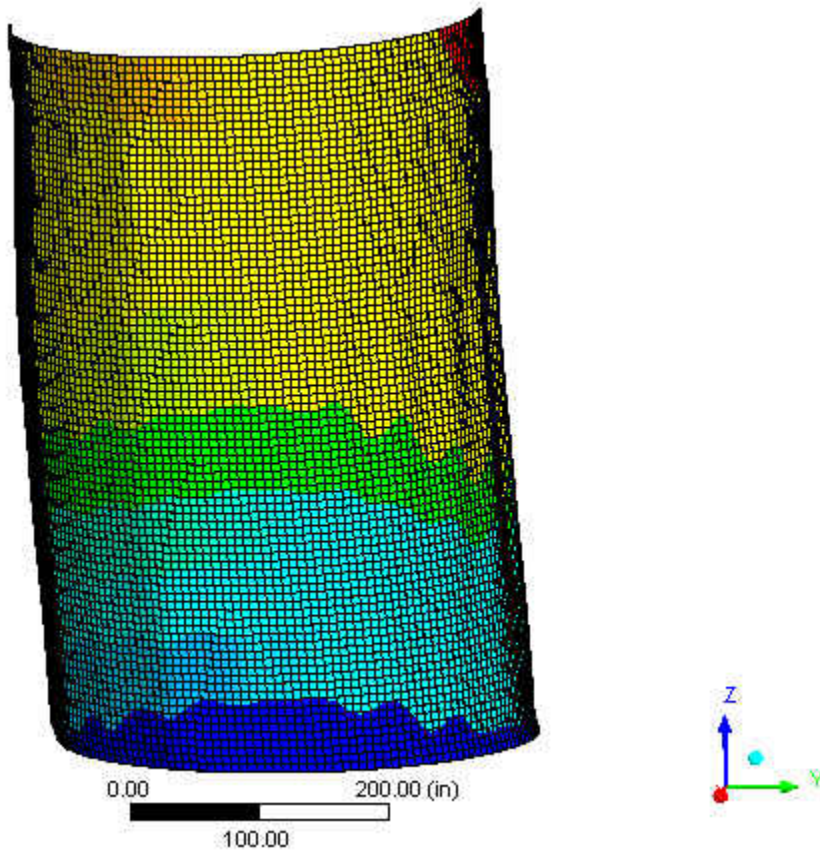


Figure 67: Shell Deformation of Model 10

Model 11

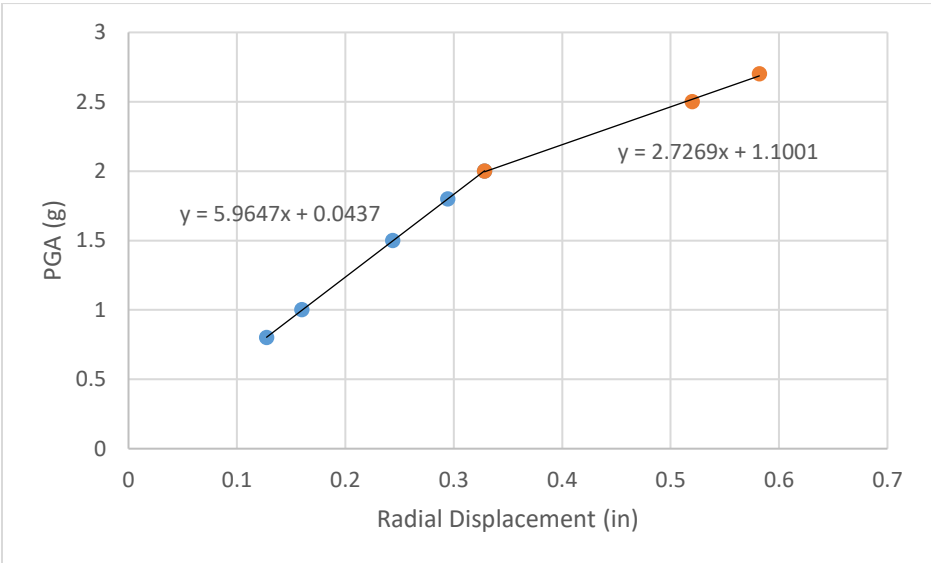


Figure 68: Pseudo Equilibrium Paths for the Critical Node of Model 11

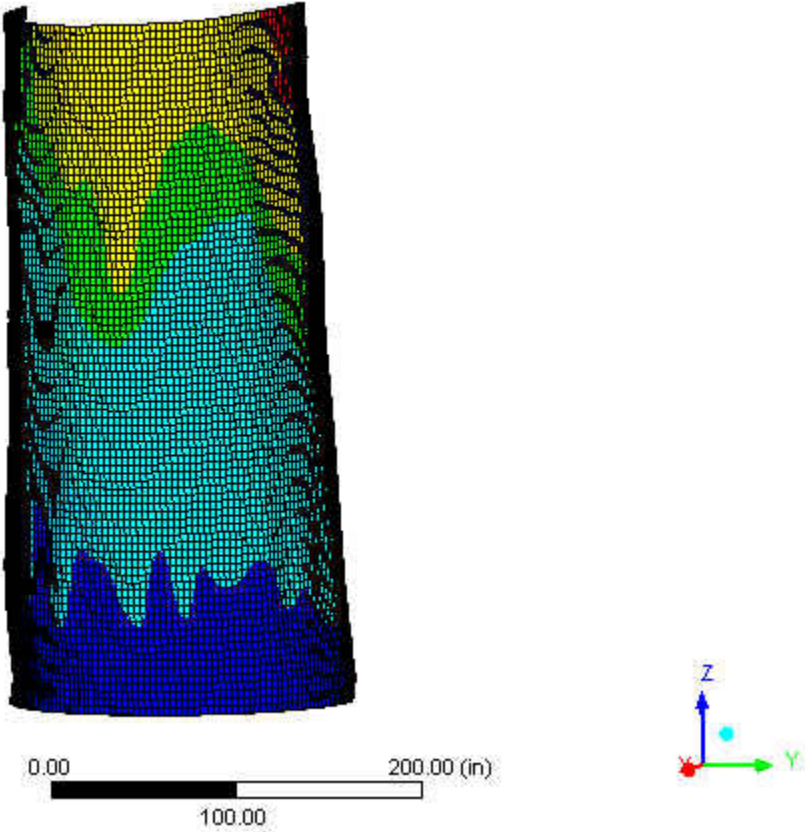


Figure 69: Shell Deformation of Model 11



# Model 12

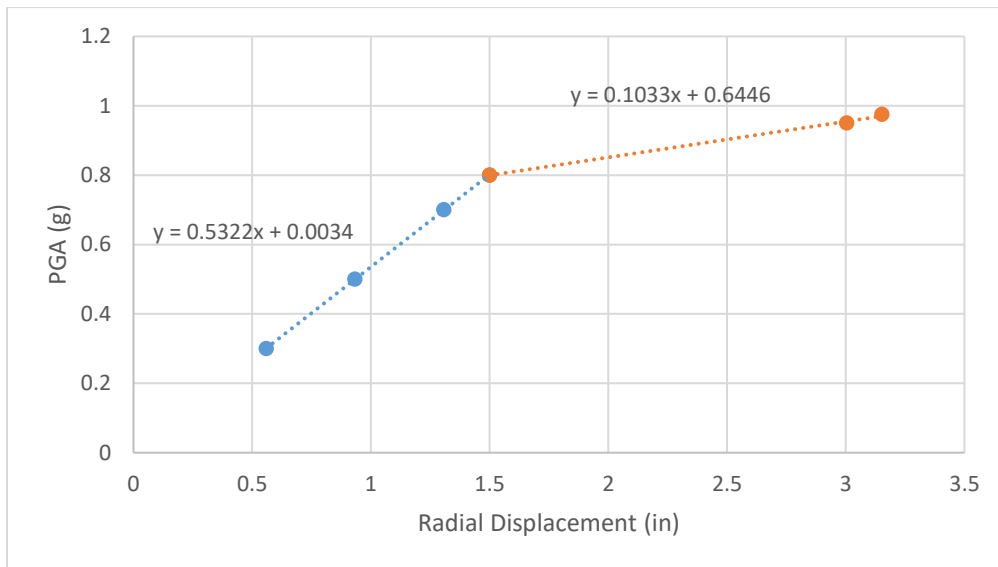


Figure 70: Pseudo Equilibrium Paths for the Critical Node of Model 12

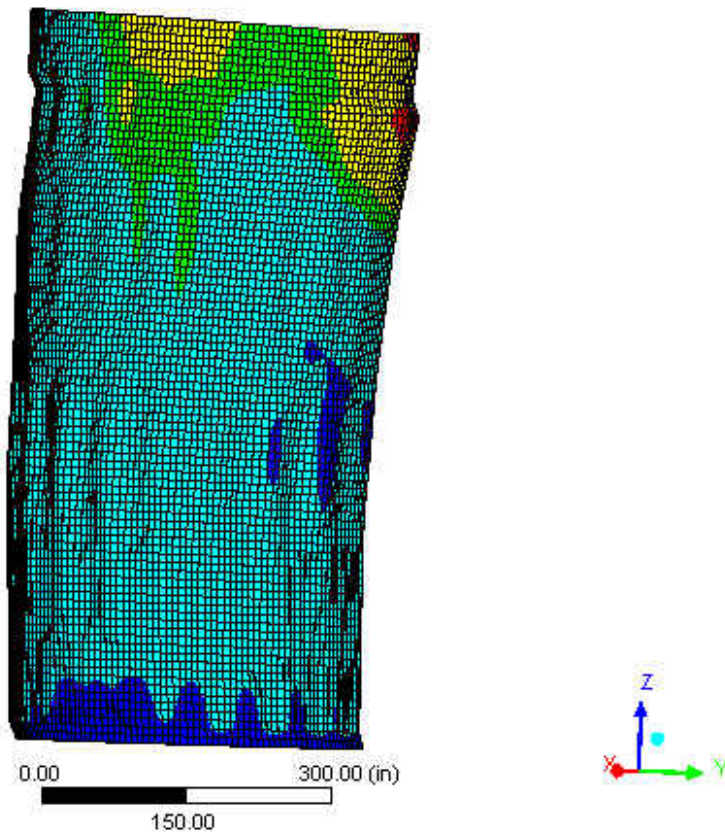


Figure 71: Shell Deformation of Model 12

## CHAPTER VII: CONCLUSION

During this research, twelve liquid cylindrical storage tanks were studied to determine the static and dynamic buckling loads. The geometries of the cylindrical tanks were analyzed with height-to-diameter ratios of 0.5, 0.75, 1.0, 1.25, 1.5, and 2.0, diameter-to-thickness ratios of 520.83 and 1,041.67, and a constant thickness of 0.36 inches. The finite element analysis of each tank was created in ANSYS Workbench, a computer program.

In order to determine if the ANSYS Workbench models were accurate, the theoretical buckling stresses were compared with the critical eigenvalue buckling stress found in ANSYS. The error between the theoretical buckling stresses and the finite element analysis models were found to be between 0.51% and 5.76%. These values meant that the models were accurate for the static and dynamic buckling analysis.

The static buckling analysis started with applying lateral loads to the cylindrical tanks, in order to find the eigenvalue buckling loads. The nonlinear buckling analysis was performed using a lateral load of approximately 90% of the eigenvalue buckling load. The eigenvalue buckling loads for each tank were then compared to the nonlinear buckling loads. The nonlinear buckling loads were found to be between 85% and 90% of the eigenvalue buckling loads.

Water was then added to the cylindrical tanks to 90% of the height of each tank. A modal analysis was conducted to find the mode shapes and the natural frequencies of each cylindrical tank. The first natural frequency for each tank was used to find the damping coefficients and input into ANSYS to create a transient dynamic buckling analysis for each model. The cylindrical tanks were subjected to the earthquake accelerations of the El Centro earthquake.

The dynamic buckling analysis for each cylindrical tank was completed to determine and compare the buckling behaviors of each tank. Analysis of the results show when either the height-to-diameter ratios or the diameter-to thickness ratios increase, the dynamic buckling loads of the cylindrical tanks decrease.

## REFERENCES

ANSYS® Academic Research Mechanical, Release 19.1

Butnaru, Bogdan Alexandru, et al. “The Comparative Analysis of Hydrodynamic Pressures in Cylindrical Tanks.” *Mathematical Modelling in Civil Engineering*, vol. 12, no. 3, 2016, pp. 1–12., doi:10.1515/mmce-2016-0009.

Chen, W.F., and E.M. M. Lui. *Structural Stability: Theory and Implementation*. PTR Prentice Hall, 1987.

Chopra, Anil K. *Dynamics of Structures: Theory and Applications to Earthquake Engineering*. 4th ed., Pearson/Prentice Hall, 2012.

Djermene, M., et al. “Dynamic Buckling of Steel Tanks under Seismic Excitation: Numerical Evaluation of Code Provisions.” *Engineering Structures*, vol. 70, 2014, pp. 181–196., doi:10.1016/j.engstruct.2014.03.037.

Ghosh, A. K., et al. “Aircraft Performance, Stability, and Control with Experiments in Flight.” *Stability and Control - Discussion on Equilibrium, Static and Dynamic Stability*. 2019, nptel.ac.in/courses/101104007/11.

Housner, George. (1963). The Dynamic Behavior of Water Tanks. *Bulletin of the Seismological Society of America*. 53.

Jerath, Sukhvarsh, and Mark Lee. “Stability Analysis of Cylindrical Tanks under Static and Earthquake Loading.” *Journal of Civil Engineering and Architecture*, vol. 9, no. 1, 2015, doi:10.17265/1934-7359/2015.01.009.

Mandal, P, and C.R Calladine. “Buckling of Thin Cylindrical Shells under Axial Compression.” *International Journal of Solids and Structures*, vol. 37, no. 33, 2000, pp. 4509–4525., doi:10.1016/s0020-7683(99)00160-2.

Meskouris, Konstantin, et al. “Seismic Analysis of Liquid Storage Tanks.” *Bouwen Met Staal*, 2011, tc.bouwenmetstaal.nl/publicaties\_serve.lasso?id=1581.

Roopkumdee, Wiriyaichai, and Sukhvarsh Jerath. “Buckling of Liquid-Filled Steel Storage Tanks under Earthquake Loading.” *University of North Dakota*, ProQuest, 2017, pp. 1–119.

“SHELL 181.” *SharcNet*, 29 June 2015, www.sharcnet.ca/Software/Ansys/16.2.3/en-us/help/ans\_elem/Hlp\_E\_SHELL181.html.

“SOLID 186.” *SharcNet*, 29 June 2015, [www.sharcnet.ca/Software/Ansys/16.2.3/en-us/help/ans\\_elem/Hlp\\_E\\_SOLID186.html](http://www.sharcnet.ca/Software/Ansys/16.2.3/en-us/help/ans_elem/Hlp_E_SOLID186.html).

Timoshenko, Stephen, and S. Woinowsky-Krieger. *Theory of Plates and Shells*. McGraw-Hill, 1959.

University of Berkley. “The Earthquake Engineering Online Archive.” *Library | Pacific Earthquake Engineering Research Center*, Regents of the University of California, 2016, [peer.berkeley.edu/library](http://peer.berkeley.edu/library)

Zama, Shinsaku. “Damage and Failure of Oil Storage Tanks Due to the 1999 Kocaeli Earthquake in Turkey and Chi-Chi Earthquake in Taiwan.” *Journal of High Pressure Institute of Japan*, vol. 41, no. 2, 2003, pp. 79–86., doi:10.11181/hpi.41.79.